Journal of Materials Chemistry C

ROYAL SOCIETY OF CHEMISTRY

REVIEW

View Article Online
View Journal | View Issue

Cite this: J. Mater. Chem. C, 2025, 13, 7438

Quasi-ordered photonic glass materials: fabrication strategies, performance enhancement and applications

Qilin Guo and Changchun Wang *

Received 29th December 2024,
Accepted 11th March 2025

DOI: 10.1039/d4tc05485g

rsc.li/materials-c

Photonic glass materials have drawn significant attention in emerging applications owing to their unique structural features with pseudo isotropic photonic bandgaps, short-range order and angular-independent coloration. In this review, we systematically summarize a variety of common fabrication strategies based on colloidal nanoparticles for photonic glasses and their promising applications. In particular, inverse photonic glassy pigments are discussed for improving saturation and purity of quasi-crystalline structural colors. Additionally, the role of inorganic semiconductor particles with a high refractive index upon increasing the dielectric constant for producing non-iridescent photonic materials is described. Finally, this review analyses the critical challenges and highlights the promising new areas of photonic glass materials for future applications.

1. Introduction

The precise manipulation of light–matter interactions in the diverse and sophisticated well-defined nano- and macrostructures of creatures in nature leads to highly engineered optical systems for unique visual appearance.[1–4] This kind of coloration is the consequence of fundamental optical processes of constructive interference of light diffraction, reflection or scattering by the optically designed structures at various length scales, which are known as structural colors.[5–14] Learned from nature, bioinspired designs of photonic multifunctional structures have been progressively created on the order of the wavelengths of visible light, enabling fascinating advanced optical properties.[15–27] Generally, structural colors can be categorized into non-iridescence or iridescence, which is mainly determined by the physical structural arrangement. Specifically, photonic crystals (PCs) with periodic long-range ordered arrays offer complicated photonic bandgap structures for anisotropic optical responses, indicating strong angle-dependence (Fig. 1a).[28–30] When introducing short-range order in the photonic structures, the coherent scattering of isotropic amorphous arrays dominates the macroscopic coloration resulting in angular-independent appearance, referred to here as direct photonic glasses (PGs) (Fig. 1b).[31–38] Such interesting studies on manipulating nanostructure arrangement for striking coloration have also found inspiration from analogous non-iridescent structural colors found in various birds (Fig. 1d and e).[39] However, it is worth noting that there is a lack of emerging red photonic glass coloration in the natural world, which instead often presents blue colors (Fig. 1f), which is attributed to single-particle resonances, multiple scattering and coupling effects between particles.[40–42]

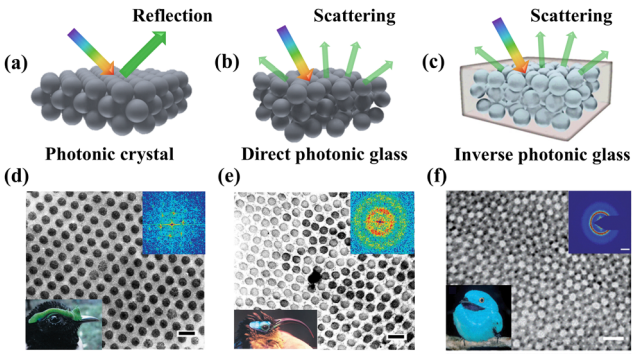

Fig. 1 Schematics of optical response in (a) photonic crystals, (b) direct photonic glasses and (c) inverse photonic glasses. Transmission electron micrograph (TEM) images of collagen arrays from (d) facial caruncles of male asities *Philepitta castanea* (lower left corner) with crystal structures and (e) male asities *Neodrepanis coruscans* (lower left corner) with amorphous structures (scale bar is 200 nm). Reproduced with permission.[39] Copyright 1999, the Company of Biologists Limited. (f) TEM images of a feather barb of the male plum-throated cotinga with sphere-type keratin and air nanostructure (lower left corner) (scale bar is 500 nm). The corresponding 2D Fourier power spectrum is shown in the upper right inset. Reproduced with permission.[43] Copyright 2009, the Royal Society of Chemistry.

State Key Laboratory of Molecular Engineering of Polymers, Department of Macromolecular Science and Laboratory of Advanced Materials, Fudan University, Shanghai 200433, China. E-mail: ccwang@fudan.edu.cn

In this context, inverse photonic glasses represent a promising candidate for producing true saturated red structural colors with quasi-ordered structures (Fig. 1c).[43]

In this review, we provide a comprehensive overview on the current research progress of photonic glass materials with multiple optical properties. Firstly, we introduce colloidal nanoparticle assembly into direct photonic glasses with preparation strategies and applications. In the second section, inverse photonic glasses are developed by a template-induced assembly method and the confined self-assembly of bottlebrush block copolymers (BBCPs). This is followed by the novel prospect on constructing non-iridescent photonic materials with high refractive index (RI) structural units. Finally, we present and discuss the challenges and promising directions for the future development of photonic glass materials.

2. Optical characteristics and color generation of photonic glasses

Photonic glasses are optical materials with short-range ordered structures and non-iridescent properties formed by controlling the degree of crystallization of colloidal particles. By interfering with the interactions between monodisperse nanoparticles or using polydisperse colloidal particles, the tendency to form long-range ordered architectures is greatly suppressed and quasi-ordered colloidal arrays are produced during the assembly process. Since photonic glasses have a defective state crystal structure with a low degree of order in the lattice arrangement, pseudo photonic bandgaps with isotropic properties are formed by scattering and interference when photons pass through these amorphous arrays. Scattering of light by photonic glass structures is a complex phenomenon, in which individual particles are themselves spectrally imaged and directionally scattered due to the interactions of magnetic and electric multipoles within the particles.[40] At the same time, neighboring particles in a photonic structure can interact to cause changes in the Mie resonance.[31] In addition, short-range ordered structures with periodicity comparable to the half-wavelength itself can lead to selective scattering of light even in the absence of Mie resonance scattering by single particles.[42] For a long time, a lot of research studies have been carried out on photonic glasses in nature, and at one time it was believed that this type of structural color was produced due to incoherent scattering of visible light by air cavities inside the material.[32] However, as the research has deepened and the theory has matured, it has gradually become the mainstream view that structural color is produced through the scattering of/interference with light caused by short-range ordered structures with isotropic spatial distributions, which disproved the long-held inaccurate view that the color is produced by incoherent scattering such as Rayleigh scattering or Mie scattering.[33] Through Fourier analysis, it can be further demonstrated that the photonic glass that produces coherent scattering and non-iridescent color effects has short-range ordered structural features. As shown in Fig. 2a, in the closely packed amorphous

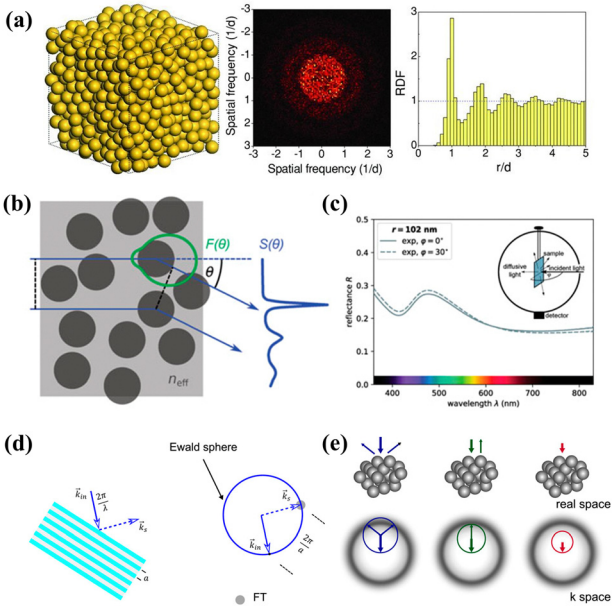

Fig. 2 (a) Schematic of a 3D PG consisting of random-close-packed spheres (left), its Fourier power spectrum (middle), and radial distribution function (right), where *d* is the sphere diameter. Reproduced with permission.[35] Copyright 2013, Wiley-VCH. (b) Scattering defined by the Mie form factor $F(\theta)$ (green) and structure factor $S(\theta)$. (c) Adjusting the effective form factor by the effects from neighboring particles allows fitting the experimental data. Reproduced with permission.[41] Copyright 2019, Wiley-VCH. (d) Ewald sphere (blue circle) construction illustrates the Bragg condition reflection of a Bragg grating (lattice constant *a*). (e) The schematic real and reciprocal space representation of the PG structure, including Ewald sphere construction, and the corresponding illustration of the half-space reflection spectrum. The thick colored arrows stand for the incident and the thin colored arrows stand for the scattered waves, with the corresponding Ewald spheres illustrated by colored circles. Reproduced with permission.[44] Copyright 2018, The Optical Society.

structure, the 2D Fourier power spectra exhibit a circular diffraction pattern, indicating that the spatial variation of the refractive index remains essentially the same in all directions and that the structure has a certain degree of ordering. In addition, the radial distribution function corresponding to the spectra shows a clear peak at short distances. However, at relatively long distances, the radial distribution function is almost a constant, which implies that this spatial arrangement has only a short-range ordered and long-range disordered structure.[35]

So far, several theories have been proposed to account for the structure of photonic glasses. For example, Noh and colleagues demonstrated the importance of short-range correlations of structure for color appearance and proposed a model based on single and double scattering.[37] Subsequently, Magkiriadou *et al.* used a quantitative scattering model to explain how anisotropic structural colors in these specific materials arise and proposed that the color appearance is dominated by the backscattering resonance of individual particles.[42] Recently, Schertel's group developed another quantitative scattering model to verify the effect of neighboring nanoparticles in an amorphous structure

on Mie scattering, and the model predicts the intact pseudo-photonic forbidden bands and structural colors in photonic glasses. The model takes into account resonant Mie scattering, short-range positional correlations, optical near-field coupling of randomly stacked spherical scatterers, and internal reflections of the sample at the boundary. As shown in Fig. 2b and c, monodisperse PS microspheres are randomly stacked in an effective medium whose refractive index can be calculated by the energy coherent potential approximation.[41] In this process, the key to the calculation of the refractive index of the effective medium is to match the average energy density of the nanoparticles with the energy density within the medium to obtain the Mie scattering correction for individual particles, which provides an effective shape factor $F(\theta)$ for the scattering theory. In addition, the structural correlation between scatterers leads to interference between particles, which can be explained by the Percus–Yevick structure factor $S(\theta)$. As such, the combined contribution of shape and structure factors to scattering enables the prediction of isotropic photonic glasses with a specific reflection color.

Additionally, in the Ewald sphere structure derived from the first-order Born approximation theory, the wavelength dependence and direction of scattered light of photonic glass materials can be similarly predicted geometrically by analyzing the degree of overlap between the Ewald sphere and the spatially averaged Fourier-transformed (FT) distribution of the dielectric constant.[36] As shown in Fig. 2d and e, the real space possessed by colloidal particles with an amorphous array distribution is shifted from the center of the reciprocal space formed after the Fourier transform, with the radius of the Ewald sphere as the wave number of the incident light and in the negative direction of the incident wave vector, which highlights that it can be intuitively found that the formed grating structure is able to satisfy the Bragg condition.[44] For long wavelengths of light, there is no overlap between the Ewald sphere and the FT, which leads to silent light scattering. Once the wavelength of the light is short enough, the corresponding increase in the wave number produces an Ewald sphere in contact with the FT of the dielectric constant distribution, resulting in the beginning of the scattering of the light. When the Ewald sphere overlaps with the FT, the scattering intensity of the light will gradually increase, which causes the reflectivity to be shorter with the wavelength and to increase and eventually reach a saturated state. Due to the symmetry of the sphere and the isotropy of the short-range ordered structure formed by the neighboring particles, it shows the same periodicity in all directions. Consequently, the overlap between the Ewald sphere and the FT at a specific wavelength will be the same for different angles of incident light, resulting in the non-iridescence-colored reflection behavior of photonic glass materials. In addition, the shape factor in the first-order Born approximation theory is a constant function in the inverse easy space, independent of the wavelength of the incident light, which leads to this theory being a powerful tool for describing scattering in disordered structures with small refractive index contrasts over a wide range of wavelengths.[37]

3. Design and performance enhancement of direct photonic glasses based on colloidal particles

Colloidal particles assembly as a bottom-up method has been proven effective in the fabrication of non-iridescent structural colors in terms of high efficiency, large-scalable production, superior repeatability and extraordinary controllability. Through disturbing the interactions between monodisperse nanoparticles or using polydispersed colloids, the tendency for the formation of long-range order is greatly suppressed and generates short-range order during the assembly process. Besides, the incorporation of a light absorbing component would inhibit multiple incoherent scattering arising from quasi-crystalline structures, yielding enhanced color visibility and optical performance.[45,46] In this section, we elaborate several creation methods and correlate potential applications of isotropic photonic glass materials, with emphasis placed upon the formation of short-range order and special photonic properties. Although most of the creation methods for preparing photonic glasses covered in this review are similar to those for preparing photonic crystals, there are significant differences from photonic crystals due to the formation of the short-range ordered structure of photonic glasses. In addition, in order to obtain better and more comprehensive discussion and coverage of key research in the photonic glass field, a table is provided to explicitly present the strengths, limitations, and trade-offs of each creation method based on a comparison of critical parameters and representative studies (Table 1).

3.1 Evaporation self-assembly

The process of suppressing the crystallization trend of nanoparticles is important to produce quasi-ordered photonic materials *via* disturbing colloidal arrangement in the context of controlling evaporation self-assembly conditions. The drop/spin coating strategy exhibits great flexibility and simple operation on the breaking the long-range ordered sequence through adjusting the volume fraction and concentration of dispersion.[47,48] Dufresne and his workers reported the creation of biomimetic isotropic structural color films through the self-assembly of bidisperse colloidal polystyrene (PS) nanoparticles based on suspension spin-coating technology.[49] As shown in Fig. 3a and b, the obtained photonic films which were formed by disperse colloids describe the non-iridescent colors. Besides, the corresponding SEM images indicate the short-range ordered arrays. However, the whitish blue color has a low color visibility. To improve the reflectivity and saturation of photonic materials, it is a good choice to incorporate light-absorbing additives, such as carbon black (CB),[80] polydopamine (PDA)[81] or polypyrrole (PPy)[82] to reduce multiple incoherent scattering arising from amorphous structures in the photonic glass. Shi and his colleagues proposed a new method to produce high-performance amorphous photonic structures with high color visibility through evaporation self-assembly of monodisperse PS particles and natural cuttlefish ink additives by a drop-coating strategy.[50]

Table 1 Comparison of fabrication methods for photonic glasses

Fabrication methods	Typical characteristics	Advantages	Challenges	Ref.
Evaporation self-assembly	Solvent evaporation drives colloidal assembly	Low cost, scalable	Low color uniformity in large areas	47–50
Infiltration-assisted assembly	Rapid solvent removal *via* infiltration forming short-range ordered arrays	Rapid patterning, high resolution	Substrate-dependent, high cost	51–54
Supramolecular-induced assembly	Supramolecular interactions promote colloids arrangement	Self-healing properties, tunable mechanical properties	Limited interaction strength, poor stability at high temperatures	55–58
Spray coating	Assemble into isotropic structures *via* spraying	Efficient, economical, suitable for large-scale production	Difficulty in controlling uniformity, particle aggregation	59–62
Inkjet printing	Precise deposition of colloidal particles	High resolution, low material waste, suitable for complex patterns.	Particle aggregation, poor pattern uniformity	63–65
3D printing	Printing technique for tailored structural colors with photonic inks	High precision, customizable, suitable for complex structures	Complex ink formulation, slow printing speed	66 and 67
Reverse emulsion process	Assembly of colloidal particles in emulsion droplets	Uniform superball, full-spectrum color tuning	High emulsion stability, complex preparation process	68 and 69
Microfluidic technique	Precise control of droplet size using microfluidic devices	Monodisperse droplets, tunable size	Complex device setup	70–72
Centrifugation method	Rapid assembly of colloidal particles *via* centrifugal force	Simple operation, rapid fabrication	Difficulty in avoiding centrifugation defects	73 and 74
Electric-induced assembly	Deposition of colloidal particles under an external electric field	Fast response, reversible, suitable for dynamic displays	Requires high dielectric constant particles, precise electric field control	75–78
Shear-induced assembly	Rapid assembly of colloidal particles under shear force	Rapid, effective, defect-tolerant	Limited specific structured nanoparticles	79

The difference between the PS spheres and the ink particles leads to the inhibition of long-range ordered arrangement, eventually forming quasi-ordered structures. Besides, a diverse range of non-iridescent colors from blue to red with various hues and purity can be precisely tuned through manipulating the particle diameters and the relative proportion of ink particles (Fig. 3c and d). Furthermore, these photonic materials can be processed into non-iridescent physical pigments, and even embedded into commercial resins for multi-functional vision performance (Fig. 3e and f). However, the strong Mie scattering of individual spheres in the amorphous arrays seriously affects the quality of photonic glass films. Adopting the fabrication of better short-range ordered structures or utilizing inorganic nanoparticles with higher refractive index (RI) as building blocks may provide a new direction for progressing photonic glass materials with enhanced color saturation.

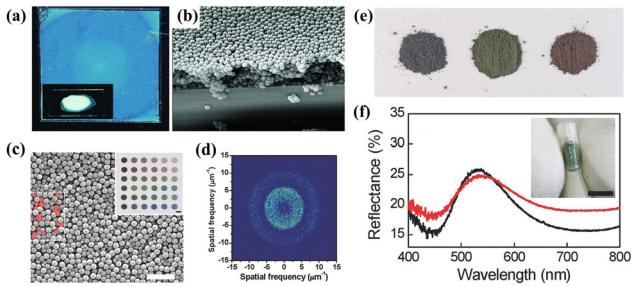

Fig. 3 (a) Photograph and (b) SEM image of a blue amorphous film with mixed 226- and 271-nm colloids. Reproduced with permission.[49] Copyright 2010, Wiley-VCH. (c) SEM image and (d) corresponding 2D Fourier transform of an amorphous pigment by 200-nm PS spheres and cuttlefish ink particles. The inset shows the color palette offered by varied PS particles. (e) Powders of three colored samples. (f) The reflection spectrum of the green powder with (red line) and without (black line) a water glue added. Scale bar is 5 mm. Reproduced with permission.[50] Copyright 2015, Wiley-VCH.

3.2 Infiltration-assisted assembly

While non-iridescent structural color materials with amorphous colloidal arrays (ACA) can be successfully obtained by controlling the evaporation kinetics of monodisperse nanoparticles in the suspensions,[51,52] the difficulty of rapid and large-scalable fabrication of high-performance structural colors with tailored full-spectrum colors remains the primary bottleneck for advanced functional applications. Duan and his colleagues proposed a universal and versatile approach for creating non-iridescent colors through liquid infiltration-assisted (IFAST) driven colloidal non-equilibrium assembly on permeable substrates for structural color printing.[53] The realization of rapid liquid infiltration lies in the well-defined substrate, *i.e.*, anodic aluminum oxide (AAO) membrane with uniform and size-controlled cylindrical pores, which enables droplets to swiftly vanish within 0.9 ms. Consequently, the colloidal crystallization is strongly inhibited so as to form an quasi-ordered arrangement (Fig. 4a and b). The isotropic structure leads to the angle-independence with the fact of remaining reflection peaks at varied incidence angles (Fig. 4c). In addition, as illustrated in Fig. 4d, the authors present a simple model for analyzing the infiltration-driven colloidal assembly, which reveals the strong Stokes drag force could disrupt the equilibrium of colloidal crystallization thus forming short-rang ordered packing. Besides, high-resolution and full-spectrum non-iridescent structural color patterns can be achieved through IFAST printing (Fig. 4e and f), offering unprecedented flexibility in fabricating desirable wide

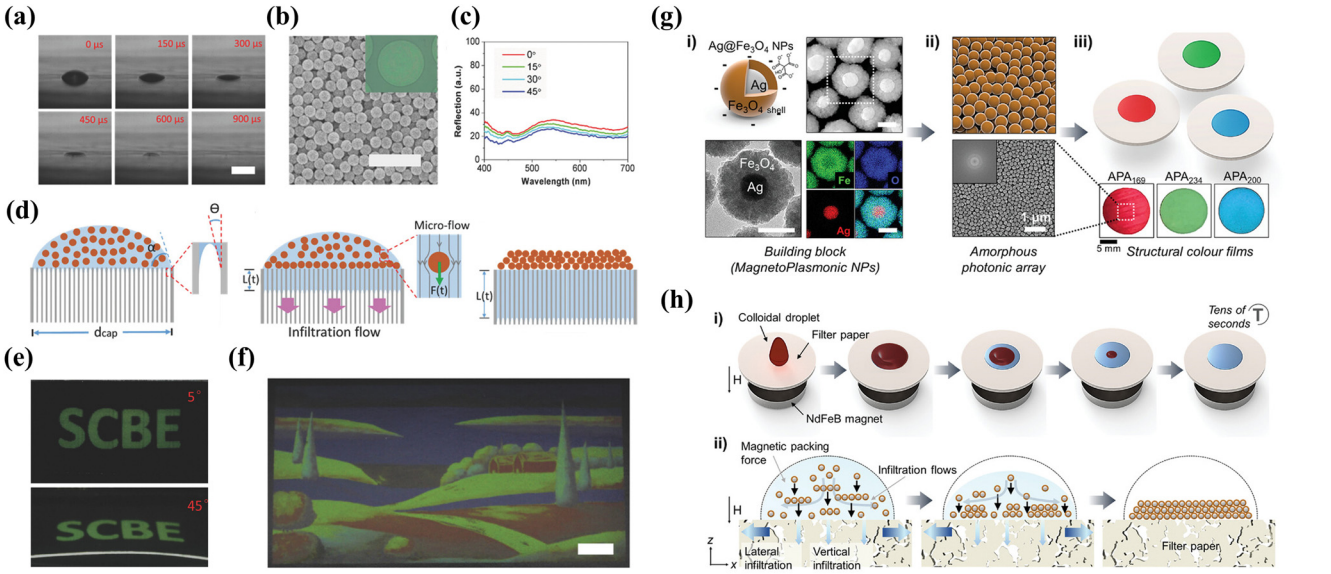

Fig. 4 (a) Images of the water droplet removal process on an AAO membrane taken with a high-speed camera. The scale bar is 100 μm. (b) SEM image of amorphous arrays. The scale bar is 1 μm. The inset shows the microscope image of printed single microdots. (c) Reflection spectrum of ACAs at varied viewing angles. (d) Illustration of the formation of ACAs with infiltration flow. (e) Photographs of inkjet printing letters at different angles. (f) A multicolored painting of a landscape. Scale bar is 1 cm. Reproduced with permission.[53] Copyright 2018, Wiley-VCH. (g) Characterization of magnetoplasmonic NPs and amorphous films. (i) TEM, STEM and EDS elemental mapping images of the Ag@Fe_3O_4 NPs. (ii) Schematic illustration and SEM image of the amorphous photonic array and corresponding 2D FFT pattern. (iii) Schematics and photographs of structural color films composed of varied-size NPs. (h) Schematic illustration of the fabrication and formation amorphous films. Reproduced with permission.[54] Copyright 2022, Wiley-VCH.

viewing-angle photonic devices with diverse tailored optical and functional properties.

Although the rapid removal of the solvent by evaporation or infiltration has been proven to be successful in suppressing the colloidal crystallization for fabricating short-range ordered arrays, it is still subjected to the limitations of solvent or substrate types. Utilizing external driving forces to rapidly arrange colloidal particles into quasi-ordered structures is a promising method for simplifying the manufacturing process. Lee *et al.* reported a novel approach called magnetic field-assisted coating technology for rapid and scalable creation of uniform amorphous photonic arrays (APAs) featuring unique structural colors composed of magnetoplasmonic Ag@Fe_3O_4 nanoparticles (MagPlas NPs) (Fig. 4h).[54] The external magnetic field promotes the MagPlas NPs rapid down infiltration to assemble for quasi-ordered structures and completely suppress the coffee-ring effect. As shown in Fig. 4g(ii), the SEM image and 2D fast Fourier transform (FFT) demonstrate the periodicity of the spatial variation of the RI is equivalent in all directions, indicating the non-iridescent characteristic of all samples. Besides, the diverse precisely tailored reflected colors with full visible spectrum of light could be readily tuned by simply regulating a variety of particle diameters, shell porosity, or thickness of the additional SiO_2 shell. Benefiting from specific narrowband resonances of Ag and broadband absorption of Fe_3O_4, the as-obtained photonic films exhibit substantially enhanced color visibility and saturation. This type of photonic material prepared from plasmonic building units possesses high RI sensitivity due to the presence of a localized surface plasmon resonance (LSPR) effect and photon plasma coupling,[83] which makes them promising candidates for full-spectrum displays, active sensors or smart devices.

3.3 Supramolecular-induced assembly

The quasi-ordered aggregation of colloidal nanoparticles can also be considered on the basis of appropriate interactions and good compatibility between particles and matrix such as supramolecular assembly.[55,56] Yao *et al.* proposed a supramolecular strategy for preparing self-healable non-iridescent organogel nanocomposites.[57] As shown in Fig. 5a, the formation of intermolecular and intramolecular hydrogen bonding between amino terminated poly(dimethylsiloxane) (NH_2-PDMS-NH_2) and isophorone diisocyanate (IPDI) promotes the generation of supramolecular crosslinked networks. With the rapid removal of chloroform solvent, the crystallization trends of the silica (SiO_2) nanoparticles become a hindrance, inducing the formation of isotropic and short-range ordered arrangements (Fig. 5b). The optical and mechanical properties of the obtained membranes can be conveniently adjusted by regulating the amount of organogel. As illustrated in Fig. 5c and d, more saturated green colors can be observed through increasing amount of the polymer gel. In addition, the introduction of polymer gel causes larger packed particle diameters ascribed to a layer of polymers wrapped on the nanoparticles (Fig. 5e and f). Thanks to the reconfiguration in polymer chains of the supramolecular gel, the photonic materials display reliable and fast self-healing capability, which has a higher tolerance to mechanical damage for maintaining the original optical quality (Fig. 5g and h). In order to obtain multi-functional photonic materials with brilliant colors and broad spectrum responsiveness,

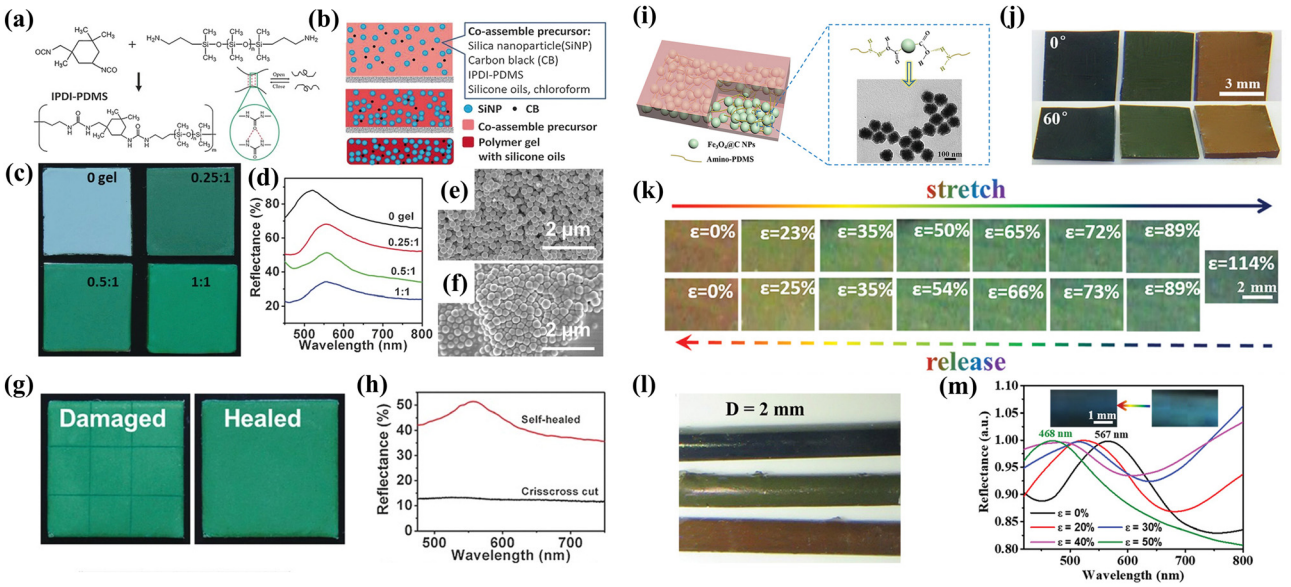

Fig. 5 (a) Synthesis of the IPDI-PDMS polymer. (b) Schematic illustration of the preparation of the self-healable nanocomposite membranes through supramolecular-induced co-assembly. (c) Photographs and (d) reflection spectrum of nanocomposite membranes with varying gel/SiNP weight ratios. SEM images of nanocomposite membranes with gel/SiNPs weight ratios of (e) 0 : 1 and (f) 0.25 : 1, respectively. (g) Photographs and (h) corresponding reflection spectrum of structural color membranes crisscross cut and self-healed. Reproduced with permission.[57] Copyright 2017, Wiley-VCH. (i) Illustration of the design of Fe_3O_4@C/PDMS PEs. (j) Photographs of photonic PEs at varied viewing angles. (k) Photographs of red-colored PEs under stretching and releasing at various strains. (l) Photographs of different colored fiber coatings. (m) Reflection spectrum and inset corresponding photographs of green fiber at different strains. Reproduced with permission.[58] Copyright 2020, Wiley-VCH.

Zhang and Zhu *et al.* developed the creation of supramolecular photonic elastomers (PEs) with angle-independence used by carbon-coated Fe_3O_4 nanoparticles (Fe_3O_4@C NPs) and amino-terminated poly(dimethylsiloxane) (amino-PDMS) polymer (Fig. 5i).[58] The exploiting of Fe_3O_4 with high RI and broad light absorption ensures the absorption capability of incoherent scattering light, improving the saturation of photonic materials. The isotropic stacked Fe_3O_4 nanoparticles and the polymer matrix with supramolecular effects not only endow the PEs with a non-iridescent characteristic, but also provide mechanochromic features similar to that of chameleon skin (Fig. 5j and k). Additionally, mechanochromic colorful coatings based on a simple dip-coating process are further produced for the demands of aesthetics (Fig. 5l and m). Therefore, the supramolecular assembly strategy provides a promising perspective on fabricating advanced photonic composites with non-iridescence and self-healing properties as potential applications including flexible electronics, visualized sensors, colorful coatings and so on.

3.4 Spray coating

Along with the requirements of preparing photonic glass materials on a large scale, spray coating synthesis has also been proven to be an efficient and economical way to accelerate the volatile solvent removal, thus facilitating the formation of short-range ordered structures.[84,85] Song *et al.* reported a facile spray-coating approach for fabricating brilliant non-iridescent structural color films in the system containing bidisperse colloidal nanoparticles and a fraction of graphene quantum dots (GQDs) (Fig. 6a).[59] Analogously, the adding of GQDs could not only absorb the strong incoherent light scattering for improving saturated structural colors, but also enhance the absorption and emission properties due to the pseudo photonic bandgap edge effect and slow photon effect to boost the brightness (Fig. 6b). In addition, the obtained photonic materials are subjected to a brilliant non-iridescent colorful humidity sensor, promoting the practical application of structural colors in switchable optical devices. On the other hand, to improve the adhesivity of most existing non-iridescent materials, Zhao and his co-workers presented a novel view on creating non-iridescent graphene oxide (GO) pigments with the desired features of self-adhesivity and brightness through a rapid spray coating method.[60] The composite elementary units were obtained by utilizing PDA and GO as the outer layer to encapsulate the SiO_2 nanoparticles to generate SiO_2@PDA@GO@PDA hybrid nanoparticles (Fig. 6c). The existence of PDA significantly increases the interaction force between the colloidal particles to induce the non-iridescent structural color coatings with typical quasi-ordered feature and vivid appearance (Fig. 6d). Furthermore, Tang *et al.* also proposed such a strategy for introducing synthesized water-borne polyurea (WPU) into the quasi-ordered structure of polysulfide microspheres (PSFMs) for preparing a non-iridescent structural color coating with high color visibility, great structural stability, and self-healing properties through spraying the mixed emulsion.[61] Fig. 6e demonstrates the feasibility of large-scale preparation of fabrics coloration, and the silk fabric still maintains relatively good integrity and unimpaired colors after the friction test (Fig. 6f and g), indicating the vast prospects for

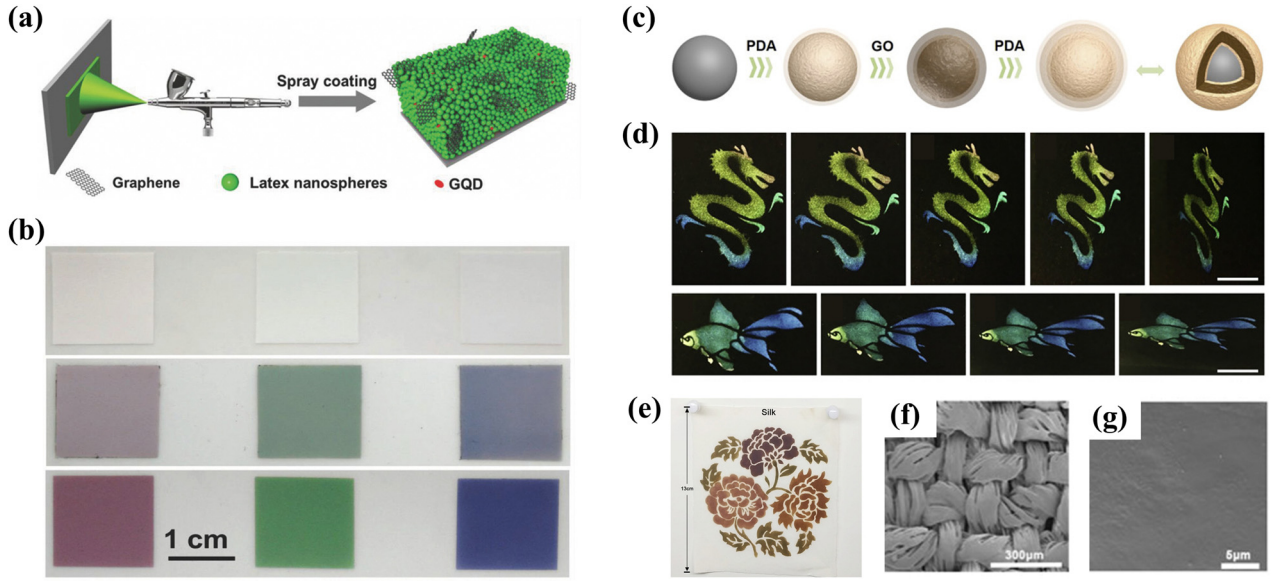

Fig. 6 (a) Schematic illustration of the fabrication process by spray-coating. (b) Photographs of non-iridescent photonic films without and with GQDs. Reproduced with permission.[59] Copyright 2018, Wiley-VCH. (c) Schematic of the generation process of SiO_2@PDA@GO@PDA hybrid nanoparticles. (d) Different patterns observed at varied angles. Reproduced with permission.[60] Copyright 2019, Elsevier. (e) Complex pattern sprayed with four different particle sizes on silk. SEM images of the pattern with a WPU/WPU film on silk (f) before and (g) after friction and washing tests. Reproduced with permission.[61] Copyright 2019, American Chemical Society.

fabricating non-iridescent structural color fabric through special customized nanoparticles using a spray coating strategy.

Beyond developing non-iridescent photonic materials with single-component building unis, co-assembly of spray coating strategies would be a more effective method to precisely tune structural colors throughout the entire visible spectrum. Recently, Wang *et al.* reported rapid fabrication of binary metastable photonic pigments through spraying bidisperse SiO_2@PDA nanoparticles.[62] During the spray process, steady-state photonic structures dominated by thermodynamics are broken by enhancing interaction forces and customizing the surface roughness of building blocks to regulate the thermodynamic and dynamic factors simultaneously. Consequently, a variety of photonic materials with angle-independence have been successfully prepared *via* adjusting the colloidal diameters (Fig. 7a–c). Subsequently, a secondary emerging structural color can be obtained through superposition of photonic bandgaps in the binary steady-state photonic system. As shown in Fig. 7d and e, inspired by the coloration mechanism of longhorn beetles, a series of binary photonic pigments were prepared by regulating the mixing ratios of building block dispersions. The obtained photonic pigments exhibit amorphous structures with short-range order but long-range disordered arrays, which is evidenced by the SEM images in Fig. 7f. The authors claimed that these binary metastable amorphous photonic pigments are a brand-new ''true color'', and they also used a 3D finite difference time domain (3D-FDTD) method to confirm the good match between the reflection spectrums of simulated structure and real photonic structure, further confirming the ''true color'' in spectroscopy (Fig. 7g). This work highlights a facile method to prepare diverse non-iridescent photonic pigments with brightness enhancement through binary colloid spraying co-assembly for realizing the tunability and multiplicity of true colors.

3.5 Inkjet printing

The effect of printing for creating high spatial resolution patterns over large areas at low cost and material usage on the visual appearance is also important in the context of additive manufacturing.[87–90] Inkjet printing, as an emerging and scalable programmable technology, can flexibly control non-iridescent structural color patterns, allowing for various high-performance applications including optical sensing, information encryption or electronic devices.[63,64,91,92] Fig. 8a and b demonstrate the illustration of self-assembling for fabricating non-iridescent hemispherical microdomes with different structural colors.[63,65] The key to achieving effective printing and successful nanoparticle alignment lies in the use of binary solvents with high viscosity and boiling point and surfactant mixtures, which produces Marangoni flow for promoting the formation of ordered structures and inhibiting the coffee ring effect. The dispersed melanin nanoparticles (MNPs) tend to crystallize when their concentrations reach a critical value with the removal of solvent. In addition, SEM images in Fig. 8c exhibit the successful fabrication of MNP microdomes. Inkjet printing provides precisely positioned individual microdomes with structural colors ranging from blue to red by only simply regulating the diameters of MNPs, in which the highly vivid colors with excellent uniformity between pixels due to a high refractive index contrast on the surface of MNPs (Fig. 8d). Besides, the authors concluded that the non-iridescent characteristic is mainly attributed to the diffusive scattering from the

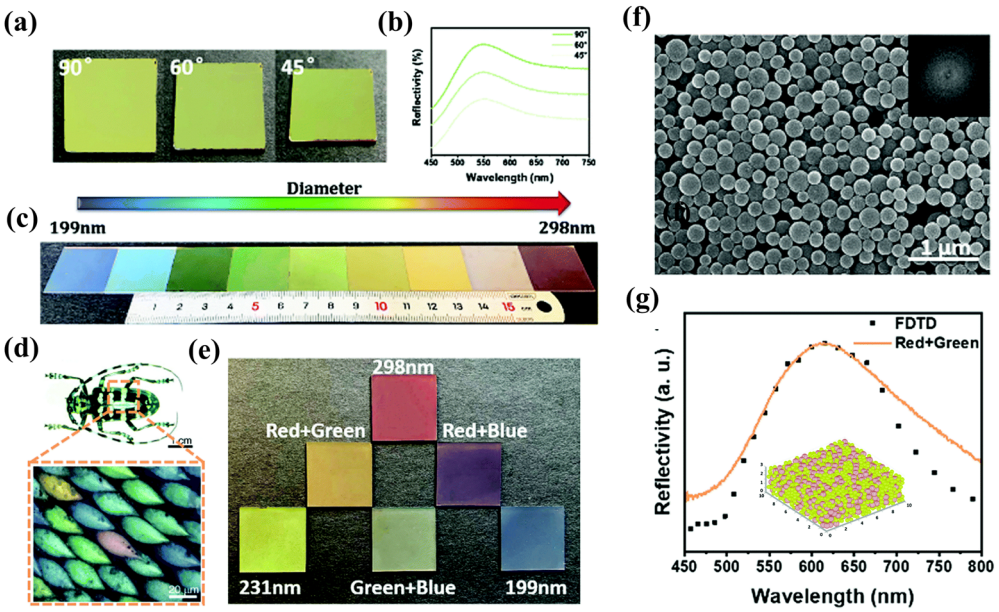

Fig. 7 (a) Photographs and (b) corresponding reflection spectrum of green colored films at different viewing angles. (c) Optical images of non-iridescent colors formed by different-sized PDA@SiO_2 NPs. (d) Optical image of longhorn beetle *Anoplophora graafi* (Coleoptera), showing an optical microscopic image of the mixed array of coloration units. Adapted with permission.[86] Copyright 2010, Optical Publishing Group. (e) Optical images of blending photonic pigments. (f) SEM image of binary photonic pigments. (g) Measured (solid line) and calculated by the 3D-FDTD method (dotted line) reflection spectrums of binary photonic pigments. Reproduced with permission.[62] Copyright 2022, the Royal Society of Chemistry.

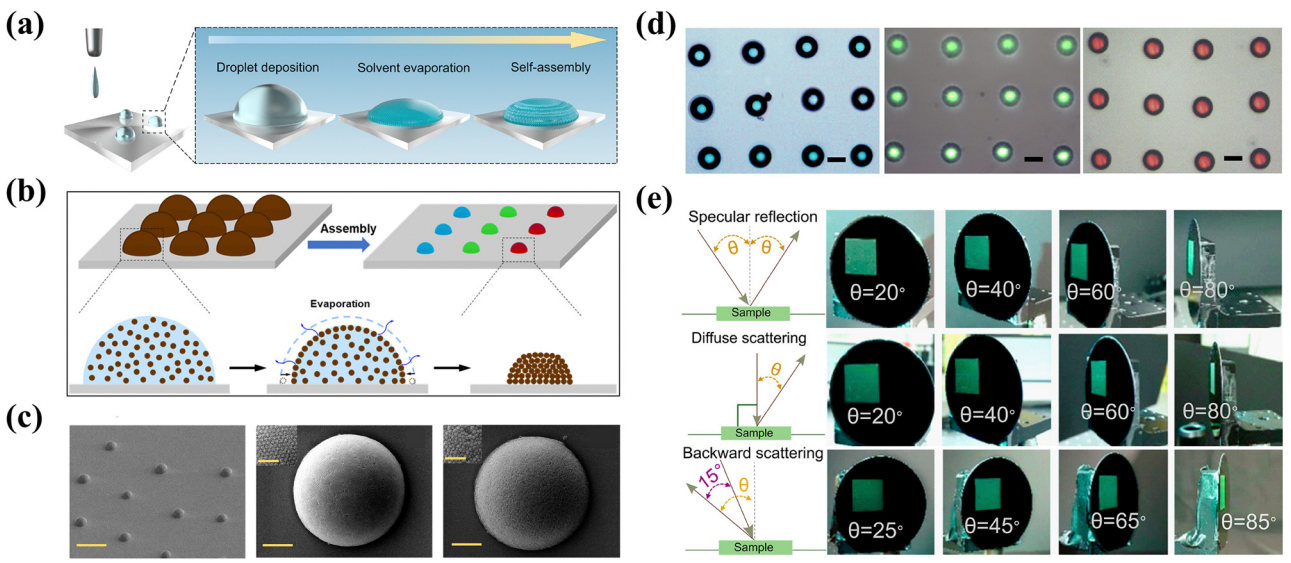

Fig. 8 (a) and (b) Schematic of inkjet printing and self-assembly of photonic microdomes. Reproduced with permission.[63] Copyright 2022, American Chemical Society. (c) SEM images of several and individual printed photonic microdomes. (d) Optical microscopy images of photonic microdomes with different particle diameters. The scale bar is 20 μm. (e) Photographs of angle-independent colors at different detection modes. Reproduced with permission.[65] Copyright 2020, American Chemical Society.

photonic domes confirmed by the fact that the same colors have varied incident angles (Fig. 8e). This strategy of preparing highly non-iridescent structural color materials through inkjet printing technology greatly alleviates the time-consuming problem of traditional self-assembly, highlighting the possibility for reproducible well-defined patterns over large areas on a variety of substrates.

3.6 3D printing

The complicated angle-independent patterns with high controllability and versatility were further investigated in more details by sophisticated 3D printing integration technology.[66,93–95] Wang and his colleagues presented a novel strategy for the facile creation of non-iridescent structural color inks through 3D printing for optical anti-counterfeiting (Fig. 9a).[67] The photonic

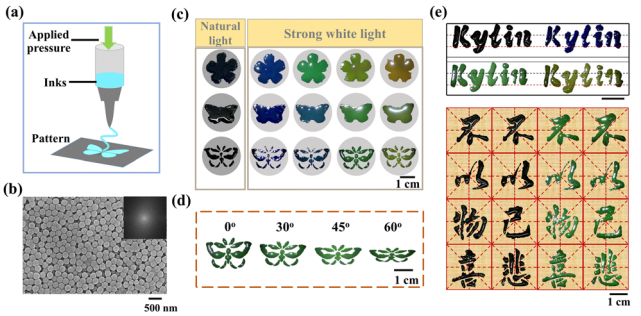

Fig. 9 (a) Schematic illustration of the creation of a butterfly pattern with the as-prepared structural color inks through 3D printing. (b) SEM image of photonic inks and the 2D FFT pattern inset. (c) The printed patterns appear black under natural light and colorful under a strong white light. (d) Photographs of photonic butterflies at varied viewing angles. (e) Optical images of the printed word "Kylin" and Chinese characters. Adapted with permission.[67] Copyright 2023, the Royal Society of Chemistry.

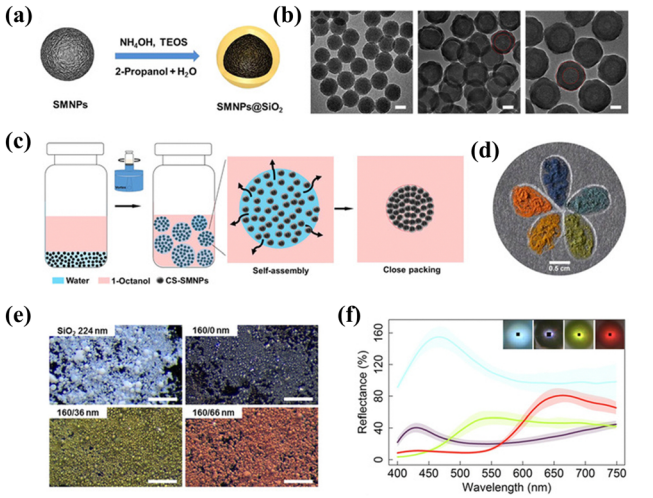

Fig. 10 (a) Synthesis process of silica-coated melanin nanoparticles. (b) TEM images of hybrid nanoparticles with different shell thicknesses. (c) The self-assembly of supraball structures *via* a reverse emulsion process. (d) Supraball inks made of five different sizes of core–shell nanoparticles. (e) Optical images and (f) reflection spectrum of supraballs made of four types of nanoparticles: 224-nm pure SiO_2 nanoparticles and 160/0-, 160/36-, and 160/66-nm CS-SMNPs. The scale bar is 0.5 mm. Reproduced with permission.[69] Copyright 2017, American Association for the Advancement of Science.

inks were obtained by simply blending SiO_2@PDA@PHEMA nanoparticles with a soft shell and the mediated molecules of 2-hydroxyethyl methacrylate (HEMA). The powerful interparticle interaction and strong adhesive force caused by a fully swollen soft PHEMA shell can induce nanoparticles to construct short-range ordered arrays during the operation of mixing and shearing process (Fig. 9b). In addition, photonic inks with multiple tunable structural colors have unprecedented flexibility and can be produced by precisely tailoring the diameters and volume fraction of SiO_2@PDA@PHEMA nanoparticles. As illustrated in Fig. 9c–e, various shape-adjusted and customized patterns with collocations, types or styles were deservedly manufactured combined with well-designed printing procedures and special composition of photonic inks. What is interesting is that the as-prepared inks are provided with surprising optical anti-counterfeiting properties due to the strong light absorption capabilities and high blackness of PDA. Specifically, the inks or printed patterns are all black color under ambient illumination yet have a sparkling reflection coloration under strong white illumination. This work offers a straightforward insight into the scalable and high-fidelity fabrication of optical anti-counterfeiting patterns or characters with widely tunable non-iridescent structural color inks using a 3D printing technique, which is appealing for various real-life applications of selective color rendering and encrypted encoding.

3.7 Reverse emulsion process

The colloidal self-assembly in micron-scale emulsion drops has been exploited to produce three dimensional spherical structural color materials from the confined assembly systems.[68,96–98] The resultant photonic spheres with an internal hierarchical quasi-ordered nanoparticle packed architecture are independent of the rotation under illumination of a fixed incident angle of the light, which broadens their applications. However, the amorphous photonic spheres lack sufficient color saturation due to multiple incoherent scattering in the absence of absorbing materials. Xiao *et al.* demonstrated a feasible strategy for producing bright and non-iridescent melanin supraballs through a one-pot reverse emulsion process.[69] The hybrid nanoparticles composed of high-refractive index (RI) (~1.74) melanin cores and low-RI (~1.45) silica shells have a much higher reflectance than the lattice of homogeneous nanoparticles, endowing the enhanced brightness and saturation of photonic supraballs (Fig. 10a and b). The simple water-in-oil reverse emulsion template method shown in Fig. 10c briefly describes the process of self-assembly of core/shell hybrid nanoparticles into micrometer-sized photonic superballs in stable emulsified droplets, which allows for a scalable strategy for the continuous production of a large number of photon spheres. A full spectrum of non-iridescent colors with the contrast needed for a complete gamut of colors was successfully obtained by adjusting nanoparticle diameters (Fig. 10d). Besides, the authors further investigated the significant impact of high-RI core and low-RI shell on the visual appearance in Fig. 10e and f. The higher incoherent scattering of SiO_2 superballs leads to a whitish cyan color, while the strong broadband absorption in the visible spectral region of pure melanin supraballs contributes to almost black. For contrast, the photonic superballs consisting of hybrid nanoparticles exhibit highly bright and saturated olive and red colors, and the boosted reflectance appears for the consequence of the increased thickness of the silica shell. The authors also claimed that the interference effect from the short-range order is critical for the color production in supraballs made of binary core/shell nanoparticles, which has the potential for being used as replacement colorants for toxic organic- and metal-based pigments.

3.8 Microfluidic technique

In order to obtain uniform non-iridescent photonic superballs with various sizes, structure and functionalities, the emerging

microfluidic-assisted method provides a powerful platform for precisely manipulating micrometer-level control of monodisperse emulsion droplets for subsequent self-assembly.[70,71,99–103] The realization of homogenous droplets is attributed to the strong shear action of the continuous relatively dispersed phase. The nanoparticle interaction condition in the confined emulsion droplets play an important role in templating the formation of quasi-ordered structures, which affects the final optical properties. Manoharan *et al.* presented the fabrication of photonic pigments with dense quasi-ordered packings of core–shell colloidal particles using microfluidic technology (Fig. 11a and b).[72] As shown in Fig. 11c and d, the osmotic pressure gradients could induce the polystyrene/poly(nisopropylacrylamide-*co*-acrylic-acid) (PS/poly(NiPAmAAc)) core/shell nanoparticles concentrate isotropically and the structural color of pigments gradually blue-shifts from red to green due to the decrease of PS core distance. Simultaneously, the soft shell inhibits colloidal crystallization thus promoting the formation of non-iridescent photonic microcapsules with amorphous nanostructures. Consequently, the resultant green pigments exhibited brilliant colors due to the coherent scattering responsible for structural color dominates, and isotropic arrays leading to the angle-independent characteristic (Fig. 11e–g). Furthermore, diverse non-iridescent photonic pigments for the full color spectrum were prepared by controlling the average distance between the PS cores depending on the osmotic pressure difference and tuning the diameters of core–shell particles (Fig. 11h and i). In such a system, the coloration with high saturation was verified through varying the RI of the core and shell, or optimizing the ratio of the core size to the interparticle spacing, enabling the tuned length scales for suppressing multiple scattering, which offers a promising process for fabricating large quantities of non-iridescent photonic pigments based on amorphous colloidal packings.

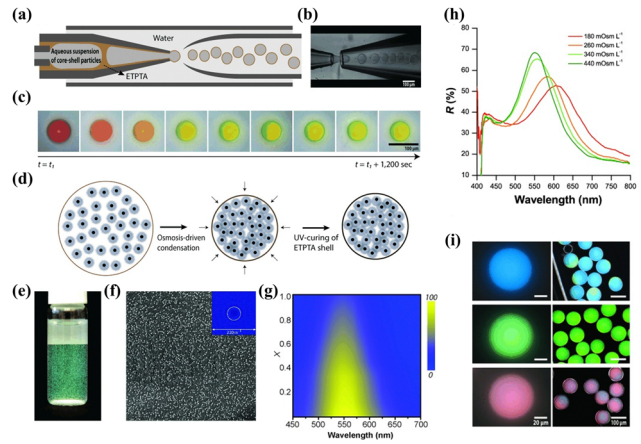

Fig. 11 (a) Schematic and (b) optical micrograph of the preparation of O/W droplets using a microfluidic device. (c) Optical micrographs of osmosis-driven condensation of droplets at 340 mOsm L^{-1} for 5 minutes. (d) Illustration of particles assembly during osmosis-driven condensation. (e) A photograph of the photonic pigments in water. (f) A cross-section SEM image of a cryogenically fractured photonic pigment microcapsule. (g) Reflectivity (yellow: 100%, blue: 0%) of a microcapsule as a function of position (x), where $x = 0$ at the center and $x = 1$ at the edge. (h) Reflectance spectra of the microcapsules equilibrated under different osmotic pressures. (i) Optical micrographs of microcapsules with different shell thickness of core/shell nanoparticles. Reproduced with permission.[72] Copyright 2014, Wiley-VCH.

3.9 Centrifugation method

The conventional centrifuge method has been shown for facile and modular assembly of colloidal particles to produce angle-independent structurally colored materials, in which the reflected coloration is due to the particle concentration in the suspension, centrifugal force, and centrifugation time.[73] Short-term centrifugation can effectively promote the formation of isotropic structures in charged particles, however, the defects in amorphous structures can generate multiple incoherent scattering to reduce the chromaticity and saturation of the obtained photonic materials. To bypass these issues, structural colors formed by biological pigments and artificial photonic assemblies were proposed.[74] As shown in Fig. 12a, bidispersed colloidal mixtures containing xanthommatin (Xa) chemically coupled to 100 nm polystyrene nanoparticles (PS100-XA) and pure PS nanoparticles of variable sizes was provided for the next rapid centrifugation to obtain colored sediment. As discussed above, the colloidal nanoparticles prefer quasi-crystalline packing owing to the polydisperse additives disrupting the long-range ordered arrays of PS colloids, resulting in non-iridescent photonic pigments (Fig. 12b–d). As predicted, a diverse range of tunable reflected colors remain original colors regardless of the incident light angles (Fig. 12e). Besides, the larger size of PS particles and higher concentration of PS100-XA led to the increased chroma and purity of red/yellow colors, indicating that color contrast was controlled by the presence of Xa while the resultant hue was regulated by the size of the PS nanoparticles (Fig. 12f and g). As such results further demonstrate that periodic long-range ordered arrays are not organized instead for short-range ordered structures with the introduction of the addition of smaller-sized particles into monodispersed colloidal particles, resulting in improved angle independence.

3.10 Electric-induced assembly

The self-assembly of dielectric colloidal nanoparticles has attracted great attention for electrophoretic color displays with better brightness and color saturation.[75,104–107] Through inducing fluidic colloidal nanoparticles deposited or concentrated on electrodes under an external electric field, the electrically responsive photonic materials exhibit the great capability of tuning structural colors with bistable state. The change in lattice constant of optical devices mainly relies on the applied voltage, deposition duration and concentration of the particle suspension. The electrically tunable full color photonic displays based on quasi-amorphous colloidal structures were reported for the first time in 2010 by Kang *et al.*[76] In this study, polydispersed Fe_3O_4@SiO_2 hybrid nanoparticles were created as high dielectric units into organic solvents for dynamic display. Large amounts of negative surface charge on the Fe_3O_4@SiO_2 nanoparticles contribute to the location on the positive electrode upon application of bias voltage, which forms the short-range ordered structures for giving rise to vivid structural

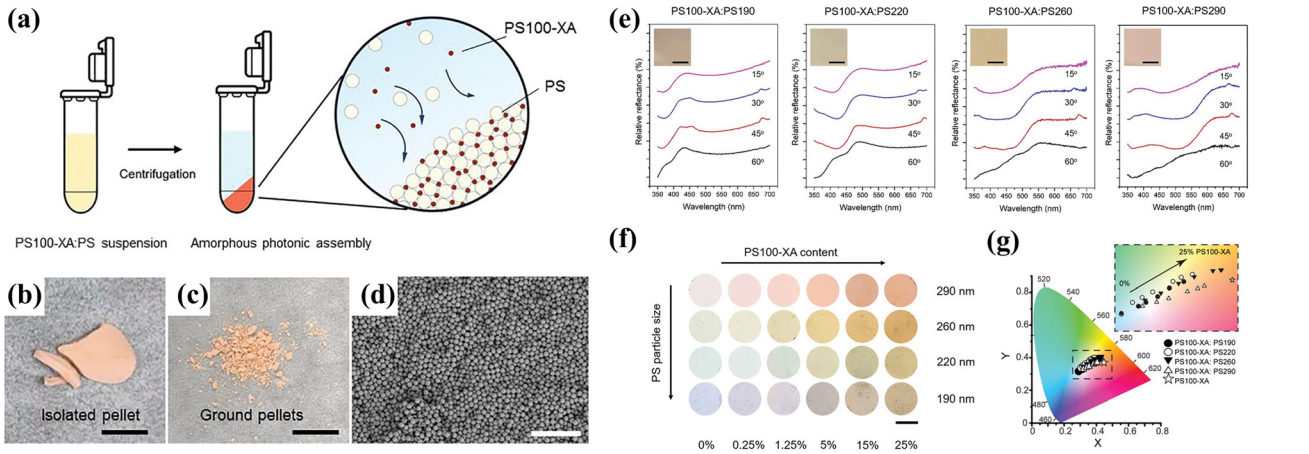

Fig. 12 (a) Illustrating the preparation of amorphous photonic materials *via* centrifuging PS100-XA:PS mixtures. (b) Photographs, (c) powers and (d) SEM images of the formed pellets. (e) Reflection spectra and photographic images of photonic materials at different incident angles. The scale bar is 2 mm. (f) Photographs and (g) CIE chromaticity diagram of photonic pigments formed by varying the size of PS nanoparticles and the amount of PS100-XA. Reproduced with permission.[74] Copyright 2021, Wiley-VCH.

colors (Fig. 13a and b). By changing the applied voltage from 1.0 to 4.0 V, the reflected colors could be tuned across the full visible spectrum from red to blue, and the color changes were fully reversible and stable (Fig. 13c and d). In addition, the non-uniform colloidal particles with high concentration could effectively suppress crystallization so as to trigger isotropic quasi-amorphous nanostructures, which is confirmed by the constant colors and is independent of the viewing angle (Fig. 13e and f). The effect of electric fields on inducing phase transitions of colloidal nanoparticles from random fluids to quasi-amorphous structures provides a positive impact on reflective displays with low power consumption, fast response and good visibility. More flexible applications of novel non-iridescent photonic electronic displays with excellent color tenability upon the engineered quasi-ordered structures were affirmed by Kim *et al.* (Fig. 13g).[77] What was important in their study was the successful measure of interparticle distances of short-range ordered arrays using synchrotron-based ultrasmall-angle X-ray scattering (USAXS). Furthermore, the electrophoretic deposition (EPD) technique derived from the above sections was employed for preparing homogeneous vivid structural color coatings as shown in Fig. 13h, with the

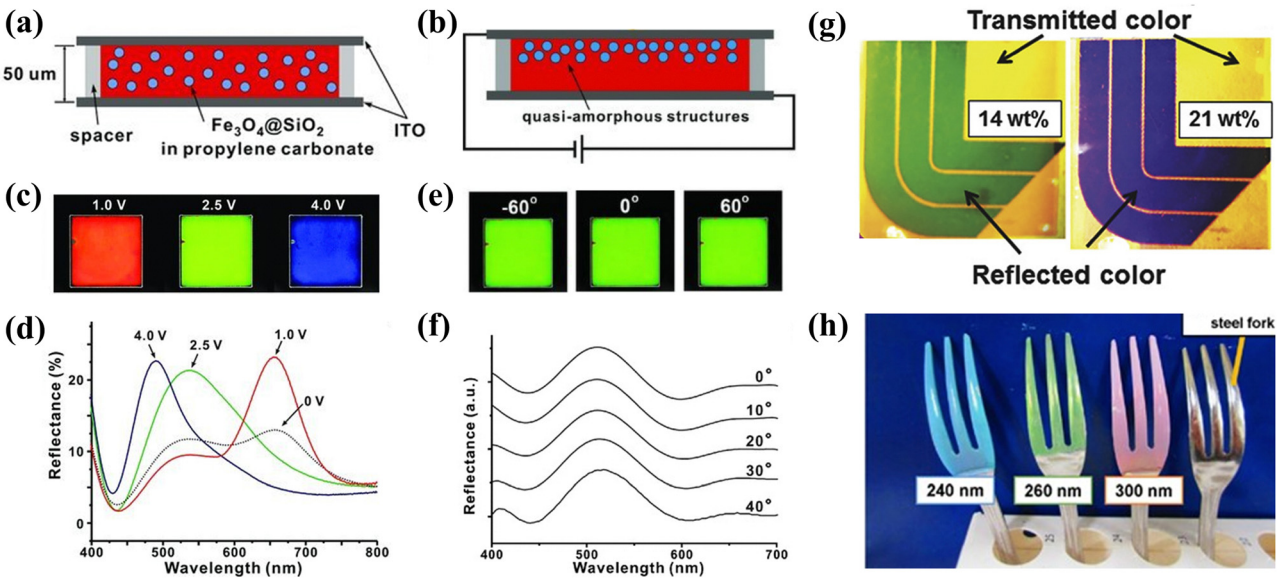

Fig. 13 Schematic structure of a photonic display pixel (a) without and (b) with an applied electric field. (c) Photographs and (d) reflection spectra of the display taken at increasing bias voltage. (e) Optical images and (f) corresponding reflection spectra of the green display at different detection angles. Reproduced with permission.[76] Copyright 2010, Wiley-VCH. (g) Photographs of Fe_2O_3/SiO_2 suspension with different Fe_2O_3 concentrations under diffusive illumination with no applied voltage. Reproduced with permission.[77] Copyright 2017, Wiley-VCH. (h) Optical photograph of the coating films prepared using different-sized SiO_2 particles *via* the EPD process. Reproduced with permission.[78] Copyright 2017, Springer Nature.

resultant amorphous packing state leading to wide-angle display materials.[78]

3.11 Shear-induced assembly

While it has been shown above that various structural colors with optimally designed micro- and nanostructures could be sufficiently investigated, it is only recently that the rapid and large-scalable fabrication process of photonic materials with time-saving, high yield and stable quality has been explored.[108–110] Since the development of bending induced oscillatory shearing (BIOS) technology, it turned out that structurally colored materials with highly ordered arrays led to tremendous progress in realizing continuous roll-to-roll mass production on a significant scale.[79] However, the shear-induced assembly of a high content of inorganic nanoparticles for constructing optical materials remains a great challenge due to the formation of nanoparticle sliding layers that need to be induced by large strain.[111,112] Wang *et al.* proposed a highly efficient one-step assembly strategy, the so-called molecule-mediated shear-induced assembly technique (MSAT), taking the core/shell magnetite hybrid Fe_3O_4@P(HEMA-*co*-EA) nanoparticles as building blocks and HEMA as mediated molecules for the facile creation of non-iridescent structural color films and pigments with high saturation and brightness under room temperature (Fig. 14a–c).[113] The multiple tunable structural colors of photonic films were obtained by precisely tailoring the sizes of Fe_3O_4 composite nanoparticles (Fig. 14d and e). In addition, the powerful MSAT allows the non-uniform magnetite nanoparticles to radially move and rapidly assemble into closely packed quasi-order 3D spatial structures, which is confirmed by the fact that the 2D FFT patterns exhibited dispersion rings with symmetric features for the spatially isotropic structures (Fig. 14f). These photonic materials could be further processed into non-iridescent photonic pigments making them feasible for applications as paints or coating (Fig. 14g). Remarkably, the non-iridescent pigments formed by close-packed nanoparticles unexpectedly possess magnetic coupling in confined quasi-ordered space for enhanced microwave absorption performance (Fig. 14h and i). This work developed a universal technical protocol for the preparation of photonic materials with inorganic nanoparticles, promoting the prospects of new camouflage materials covering the visible, infrared and radar bands.

4. Recent advances in inverse photonic glasses

Despite these advancements in fabricating direct photonic glasses, it still remains a big challenge to realize artificial rather than saturated red structural colors for larger wavelengths with disordered and short-range ordered structures. The current mainstream research believes that the production of non-iridescent red color arises from single-particle resonances,[42] however, ignoring multiple scattering and coupling effects between particles.[40,41] It is noteworthy that both form factor

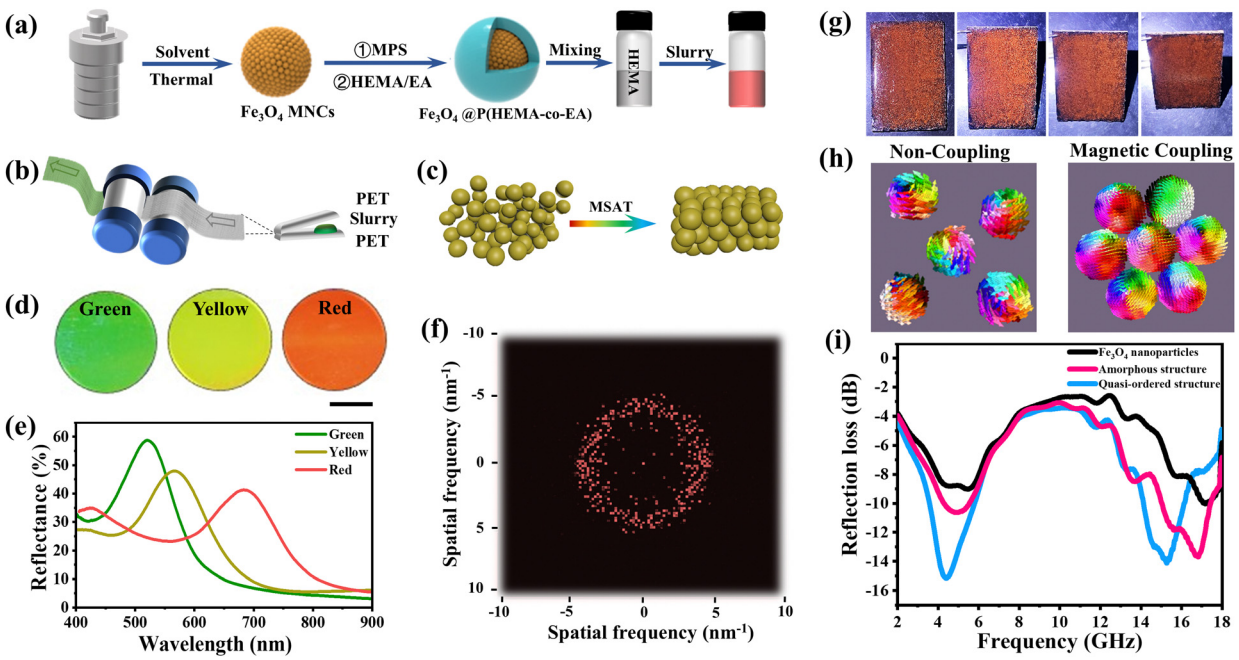

Fig. 14 Illustration of (a) the composed slurry prepared by Fe_3O_4@P(HEMA-*co*-EA) core/shell nanoparticles, (b) the fabrication process of structural color film by rolling-lamination and (c) the formation of the composite nanoparticle array. (d) Photographs and (e) corresponding reflection spectra of structural color films. (f) 2D FFT diagram of the yellow film according to the SEM image. (g) Photographs of the cured coating at various viewing angles. (h) The micromagnetic simulation for Fe_3O_4 nanoparticles with non-coupling and magnetic coupling. (i) Reflection loss (RL) curves of pure Fe_3O_4 nanoparticles, pigments with amorphous structures and photonic crystal pigments with quasi-ordered structure. Adapted with permission.[113] Copyright 2024, Elsevier.

and structure factor should be considered to analyze scattering in the photonic glass materials. The form factor refers to the individual particle properties such as size, shape or refractive index while structure factor is primarily determined by the interparticle distance or structural correlations.[114] Although the larger size of colloidal nanoparticles contributes to the increased average interparticle distance that induces the structure factor for higher-order resonant mode, simultaneously enhancing the form factor for Mie resonance peak red-shifts. As such, a second diffraction resonance peak appears in the blue visible region, which leads to a mix of structural color of blue and red.[115] How to enhance the dominance of structure factor while reducing the proportion of form factor should be considered. In contrast, inverse photonic glasses offer a novel prospect on fabricating optimal red colors through lowing the refractive index of particles that could reduce the optical path length of light traveling and the role of multiple scattering.[116] This indicates a low-refractive index in inverse PGs tends to sufficiently suppress the form factor located in the ultraviolet (UV) region, and result in pure and saturated red colors in favor of structural factor contributions. The optical response of inverse PGs is the consequence of both coherent scattering and Mie scattering induced by the short-range order associated with isotropic correlated nanostructures. Hitherto, several methods have been developed for creating inverse photonic glass materials combining the purity and saturation advantages of coloration.[117–120] Here, more attention is paid to the fabrication of such systems exhibiting isotropic structural colors focusing on the promising candidates including the template-induced assembly method and the confined self-assembly of bottlebrush block copolymers (BBCPs).

4.1 Inverse photonic glasses based on colloidal particles

In 2017, Yi and his co-workers presented an approach to fabricate disordered optical materials with angle-independent red structural colors through introducing binary hollow SiO_2 nanoparticles with the same core size but different shell thickness for amorphous arrays templating for filling polymers to construct inverse glassy colloidal structures (Fig. 15a).[121] As shown in Fig. 15b, red inverse photonic glass films were created upon infiltration with trimethylolpropane ethoxylate triacrylate (TMPEOTA) in photonic glass films with green colors, and a similar change was observed in the blue glassy films. These added polymers are index-matched to the sphere shells, which ensures the structure factor contribution dominates *via* minimizing the form-factor weight on the overall optical response. In addition, SEM images clearly demonstrated the disordered pores in the homogenous glassy structures, indicating the formation of short-range ordered structures (Fig. 15c). It is precisely these spatial isotropic amorphous arrays that endow the inverse photonic glass films with a non-iridescent characteristic with angle-independency of the reflection color and intensity (Fig. 15d). Although using colloidal nanoparticles as a template for preparing inverse photonic glass materials has been proven to be a feasible strategy, several significant challenges and issues such as synthetizing particles with specific

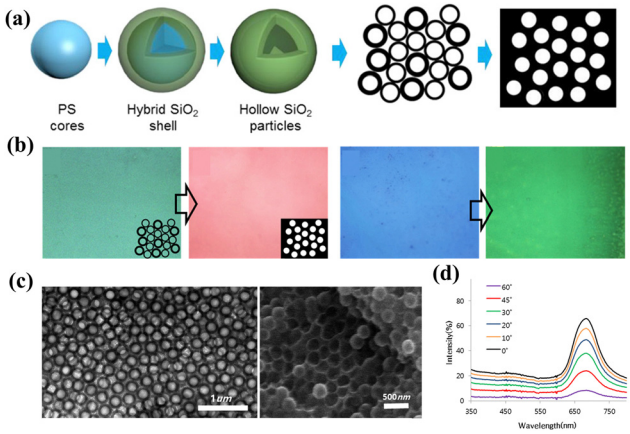

Fig. 15 (a) Synthetic route for the fabrication of hollow silica spheres from PS spheres and inverse photonic glassy structures. (b) Optical images and (c) SEM images of colloidal glass film transitions to composites with TMPEOTA for inverse glassy films. (d) Reflection spectra of red inverse photonic glass films at various viewing angles. Reproduced with permission.[121] Copyright 2017, American Chemical Society.

sizes and morphologies, controlling the arrangement and packing of colloidal particles for the desired photonic bandgap, the choice of materials and their refractive indices, and even scaling up the synthesis processes should be investigated for advancing the development of high-performance inverse photonic glasses. In this context, other promising methods including the confined self-assembly of BBCPs have been exploited as a processing candidate with compatibility between rapidly facile large-scalable production and preserving the quality and reproducibility for specific optical responses.

4.2 Inverse photonic glasses based on the self-assembly of BBCPs in confinement

Self-assembly of block copolymers (BCPs) in confined microscale emulsion droplets is of great interest in producing a variety of novel photonic materials with diverse shapes and nanostructures.[122–132] In particular, professor Dong-po Song proposed a one-step method that is a so-called organized spontaneous emulsification (OSE) mechanism to prepare inverse opal photonic pigments using amphiphilic bottlebrush block copolymers as the surfactants.[133–137] The well-defined amphiphilic BBCPs were obtained through sequential ring-opening metathesis polymerization (ROMP) utilizing a third-generation Grubbs catalyst, which features precise controlled molecule weight and a low polydispersity index. In addition, bottlebrush amphiphiles should hold two clearly distinguished hydrophobic (such as PS, PDMS, PCL, PLA) and hydrophilic (such as PEG, PVA) blocks, where the Flory–Huggins interaction parameter between them must be sufficiently large for enabling suitable interfacial tension to promote BBCPs strongly absorbing onto the water/oil interface for thermodynamically stabilizing water-in-oil-in-water (W/O/W) multiple emulsions. Eventually, ordered porous microspheres were produced with a hydrophobic block as the skeleton and uniform droplets stabilized by a hydrophilic block as pores after the removal of

solvent. Additionally, the nanopore size is significantly determined by the length of the hydrophilic block backbone, which is attributed by the fact that enhanced hydrophilicity and more hydration would result in a smaller spherical curvature of the internal water droplets, yielding larger pores within the microparticles. The coloration in these inverse photonic spheres is dominated by structural correlations, that is, the reflection position highly corresponds to the Bragg's law.

While it has been shown above that a thermodynamically favorable process evolved by BBCPs confined self-assembly could readily fabricate an inverse photonic glass microsphere, the impact of shear force applied for the rapid formation of kinetically arrested short-rang ordered porous arrays has also been explored.[138] As shown in Fig. 16a, a typical amphiphilic PS-*b*-PEO BBCP with low molecule weight (M_W = 290 kDa) was used to stabilize a homogenized emulsion with shear force thus forming internal nanoscale droplets. The tunable reflected coloration is mainly manipulated by precisely varying emulsification conditions such as the speed or the duration of the homogenization step, specifically, a higher shear force leads to larger internal pores, which is consist with their red-shifted macroscopic optical appearance and the microscopic photograph of an individual microsphere (Fig. 16b–d). SEM images further convey the existence of a highly isotropic porous architecture with short-range order, which is confirmed by the consistent green colors at the entire varied angular range (Fig. 16e). This work provides a straightforward method for the creation of libraries of non-iridescent photonic pigments with inverse glassy structures only regulating the magnitude of shear force using a well-defined and relatively low-MW BBCP in a readily and scalable manner, enabling broad viewing angles and stability required for the progressive applications.

Additionally, "thermal annealing" was also employed for fabricating inverse photonic glasses with tunable structural colors.[139] Vignolini and her colleagues disclosed how annealing can affect the migration of polymer chains and pore changes of photonic microspheres. Biocompatible PDDLA-*b*-PEG BBCPs were placed in the confined emulsification droplets and assembled into homogeneous micelles firstly, and then densely packed porous arrays were generated with the removal of toluene solvent. Subsequently, an additional thermal annealing step was applied to increase molecular mobility for further water uptake thus swelling the formed pores (Fig. 16f). Besides, the red-shift of the obtained photonic microparticles increased rapidly when treated at high temperature, which was confirmed by an evident increase of the pore diameter (Fig. 16g and h). This interesting behavior is attributed to the special thermal properties of PDLLA homopolymer, which has a glass transition temperature (T_g) of 54 °C. The higher processed temperature endows the softening polymer chain with increased mobility,

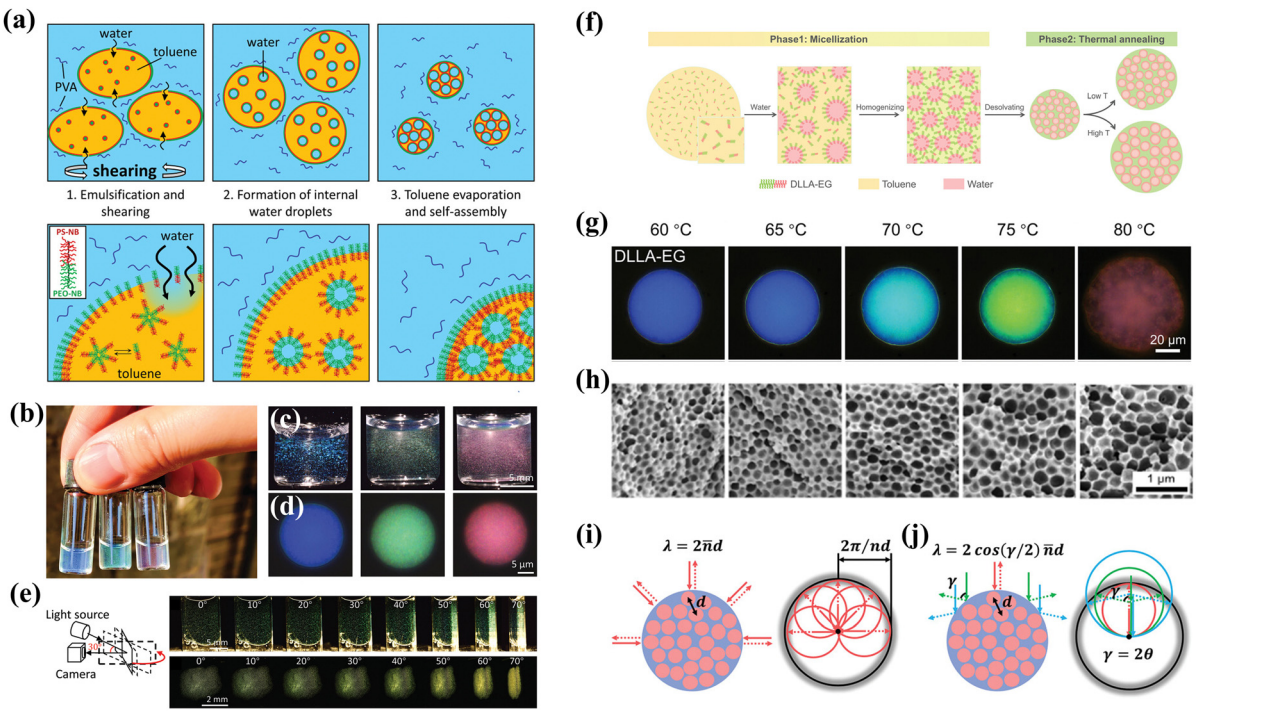

Fig. 16 (a) Illustration of the formation of inverse photonic pigments *via* forming W/O/W double emulsions stabilized by the amphiphilic P(PS-NB)-*b*-P(PEO-NB) BBCPs. (b) and (c) Photographs and (d) reflective optical micrographs of microparticles dispersed in an aqueous phase. (e) Angular-dependent macroscopic photographs of the obtained inverse photonic pigments. Reproduced with permission.[138] Copyright 2020, Wiley-VCH. (f) Schematic illustration of the formation of the inverse photonic glass structure and subsequent thermal annealing for swelling pores. (g) Microscopy images and (h) SEM images of individual microparticles prepared with DLLA-EG at different annealing temperatures. Reproduced with permission.[139] Copyright 2022, Wiley-VCH. (i) Schematic of angular dependence of the optical response under different illumination conditions for photonic glass with the Ewald's sphere. Reproduced with permission.[8] Copyright 2021, Wiley-VCH.

resulting in the bottlebrush surfactants rearranging to adapt to stabilize more water droplets into the internal emulsion with smaller spherical curvature. This also explains the key role of the high molecular mobility of the polymer matrix in the thermally induced expansion of pores. To better understand the optical response of inverse photonic nanostructures, the authors utilized Ewald's sphere to deduce the reflection position response to the incident angles under different illumination conditions.[140,141] As shown in Fig. 16i, the largest wavelength could reflect back from all directions when the inverse photonic glass was under diffuse illumination, which indicates the equivalent spatial reflection response, yielding a non-iridescent appearance across the entire viewing angles. On the other hand, a single direction illumination would induce light dispersing or scattering at broad angles with shorter wavelength reflecting at a higher angle for an angle-dependent response (Fig. 16j), however, inherently isotropic structures of inverse photonic glasses ensured the structural colors beyond restricting a specific light scattering regime for producing consistent optical responses.

5. The advantages of non-iridescent structural color materials with high-RI construct units

Generally, photonic crystals with highly long-range ordered periodic nanoarrays exhibit anisotropic optical characteristics, *i.e.* the periodic changes in refractive index experienced by light propagation within a crystal are different at distinct incident angles. The existence of complicated photonic bandgap structures (PBGs) in PCs offer unprecedented opportunities in constructing unique multi-functional optical materials and systems. However, low angle-dependence is essential for accurate communication and display in terms of sensing applications. Beyond directly producing quasi-ordered structures responsible for non-iridescent photonic materials, optimizing well-ordered structures with highly symmetrical geometries was also used to fabricate angle-independent colors.[142–144] Besides, the manipulation of light–matter interactions in the nanocrystal arrays with high contrast in dielectric values potentially ensures light propagation along the isotropic direction.[145] This inspires us that photonic crystals with periodic structures formed by inorganic semiconductor particles with high RI could be obtained for the desired optical isotropic property.

Wu *et al.* reported the possibility to prepare long-range ordered photonic crystal films with monodisperse polycrystalline Cu_2O spheres as building blocks for angle-independent structural colors.[146] The uniform Cu_2O nanoparticles could be achieved through a modified room temperature two-step reductive approach by regulating the reaction rate in favor of the isotropic growth of different crystal planes (Fig. 17a).[147] The evaporation induced self-assembly of mondisperse spheres spontaneously generates well-defined long-range ordered arrays in large domains with (111) planes parallel, which is illustrated by the SEM images in Fig. 17b. Interestingly, no

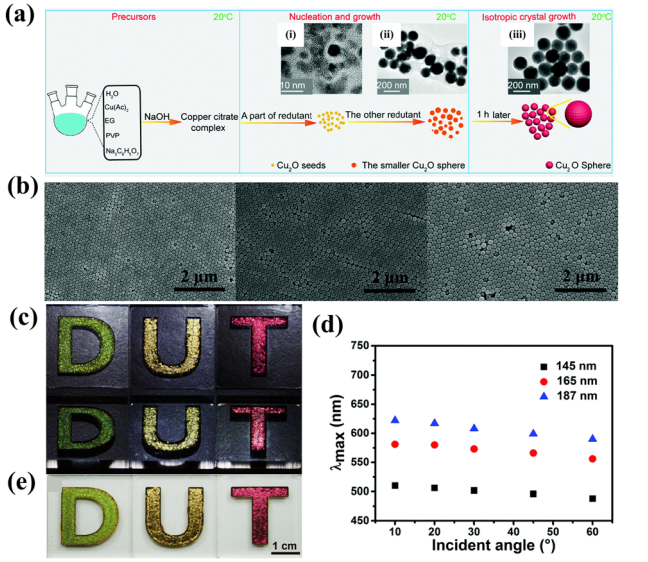

Fig. 17 (a) Schematic illustration of the preparation of monodisperse single-crystal solid Cu_2O spheres. Reproduced with permission.[147] Copyright 2019, the Royal Society of Chemistry. (b) SEM images of photonic crystal films fabricated with different-sized Cu_2O spheres. (c) Optical images and (d) corresponding reflection spectra of Cu_2O photonic crystal films at different viewing angles. (e) Digital photographs of photonic crystal films under white background and natural light. Reproduced with permission.[146] Copyright 2017, the Royal Society of Chemistry.

expected multiple Bragg scatterings were observed in these as-prepared photonic crystals with spatially anisotropic nanostructures, that is, the refractive index in spatial variation is equivalent from all orientations, which results in the constant colors of optical materials at different viewing angles (Fig. 17c and d). The effective non-iridescent structural colors are attributed from the building blocks with a high reflective index that obviously suppresses the effect of angle change on stop-band position mathematically.[148–151] Besides, the authors adopted common photonic crystals formed by SiO_2 and PS nanoparticles to further demonstrate that the building units with high refractive indices can significantly lower the angle-dependence of structural colors. Benefiting from the unique properties of Cu_2O and long-range highly ordered arrays, the obtained non-iridescent photonic crystals exhibited vivid colors taken with a white background and natural light (Fig. 17e), indicating the enormous potential and advantages of high refractive index photonic crystals in practical applications, such as in automotive paints, or in advanced photonic devices.

6. Conclusions and outlook

In this review, we have summarized recent progress in comprehensive research of diverse and multifunctional photonic glass materials including a variety of fabrication strategies, unique optical responses, and promising applications. In particular, we focus on the distinction of direct and inverse photonic glasses, in which the latter is extremely interesting as they could maximize the elimination of the form-factor effect and favor structure-factor

resonance thus improving the purity and saturation of red structurally colored glasses. Additionally, the interesting non-iridescence in photonic crystals formed by high-RI inorganic semiconductor particles are also explored and explained for exhibiting the desired optical non-iridescent property.

The advantages of photonic glasses, such as manufacturing flexibility, broadband performance, isotropic properties, reduced sensitivity to defects, and material compatibility position them as a valuable supplementary or partial alternative to photonic crystals in advancing optical technologies. Through perturbing the crystallinity of structural units during the assembly process, photonic glasses could be facilely manufactured independent on the periodicity and exhibit tremendous fascinating optical characteristics. However, this sacrifice for ordered structures would inevitably lead to an increase in multiple incoherent scattering for lowering color visibility and spectral purity. A good solution is to add a black light absorbing substance for improving color purity and saturation, yet compromising the structural color brightness in the overall visual response. By incorporating building blocks with high refractive index and good optical transparency, simultaneously adding luminescent materials such as fluorescent dyes or quantum dots can effectively enhance optical performance. In addition, through adjusting the microstructure of photonic glass, such as particle size, shape, and arrangement aiming at designing novel scattering elements, the multiple scattering and interference effects of light can be optimized for more saturated and purer colors. Additionally, with a more diverse pool of photonic glasses, greater understanding and prediction can be achieved in terms of the origin of angle-independent structural colors and the importance of short-range order correlations for the color appearance *via* corresponding scattering models,[37,41,42,152–156] which takes single-particle backscattering resonances, Mie and multiple scattering, short-range positional correlations and optical near-field coupling into account. This provides a theoretical handle for promoting high-quality photonic glass materials in practical applications.

Beyond considering the exact range of available colors, how to achieve a high saturation of red glassy colors is more challenging. The wavelength-independent of angular in direct PGs is attributed to both form-factor and structure-factor related scattering, in which the coloration can be easily achieved at an ultraviolet-blue wavelength region instead of large wavelength. By increasing the dominant role of structure-factor in the scattering process, as discussed above, the inverse PGs could significantly increase the saturation and purity of isotropic structural coloration. However, higher dimensional saturated and pure red hues are still difficult to achieve due to its intrinsic limited isotropic 3D short-range ordered structures. In this context, alternative strategies such as introducing short-range order into the hierarchical photonic films or producing novel diamond structures would be a promising space for saturated larger wavelength colors such as yellow or red glassy coloration.

Furthermore, with the improvement in people's concept of quality of life and the pursuit of a healthy lifestyle, sustainable and eco-friendly photonic glassy colors play a significant role in everyday life, from personal care to general industrial applications. Through incorporating biocompatible and environmental friendly materials (such as cellulose[157–159] or biodegradable photonic microspheres[160]) as structural units for fabricating photonic glass colorants, it has important strategic significance for the current advocacy of sustainable development and future consumables including paints, coatings or photonic pigments. Interestingly, the development of PG-based photonic pigments facilitates the viability of fabricating synthetic edible colorants with safety, stability, and diversity, enabling both a consistent coloring effect and food safety.[161,162] Looking to the future, the prospects for photonic glasses are promising, particularly in sustainable development fields such as sensors, photonics and effect pigments. As research continues to address current challenges, the development of more efficient and scalable fabrication methods will enable the realization of high-performance photonic devices. The integration of photonic glasses with emerging technologies, such as flexible electronics and nanophotonics, may lead to innovative applications and further advancements, paving the way for a new generation of optical materials.

Conflicts of interest

The authors declare no competing financial interests.

Acknowledgements

We thank the financial support by the National Natural Science Foundation of China (Grant No. 52131308 and 52373131), MOST (2022YFA1203002), and the Key research and development project of Guangdong Province (Grant No. 2020B010190003).

References

1 R. Xiong, J. Luan, S. Kang, C. Ye, S. Singamaneni and V. V. Tsukruk, *Chem. Soc. Rev.*, 2020, **49**, 983–1031.
2 S. Tadepalli, J. M. Slocik, M. K. Gupta, R. R. Naik and S. Singamaneni, *Chem. Rev.*, 2017, **117**, 12705–12763.
3 D. Gur, B. A. Palmer, S. Weiner and L. Addadi, *Adv. Funct. Mater.*, 2017, **27**, 1603514.
4 C. Zhang, D. A. McAdams and J. C. Grunlan, *Adv. Mater.*, 2016, **28**, 6292–6321.
5 Q. Guo, J. Guo and C. Wang, *Adv. Opt. Mater.*, 2024, **12**, 2401139.
6 Y. Hu, S. Yu, B. Wei, D. Yang, D. Ma and S. Huang, *Mater. Horiz.*, 2023, **10**, 3895–3928.
7 C. Duan, B. Wang, J. Li, J. Xu, J. Zeng, J. Li, Z. Zhao, W. Gao, G. Ying and K. Chen, *Small*, 2022, **18**, 2204199.
8 Z. Wang, C. L. C. Chan, T. H. Zhao, R. M. Parker and S. Vignolini, *Adv. Opt. Mater.*, 2021, **9**, 2100519.
9 Y. Ohtsuka, M. Sakai, T. Seki, R. Ohnuki, S. Yoshioka and Y. Takeoka, *ACS Appl. Mater. Interfaces*, 2020, **12**, 54127–54137.

10 G. Chen and W. Hong, *Adv. Opt. Mater.*, 2020, **8**, 2000984.
11 Y. Wang, W. Li, M. Li, S. Zhao, F. De Ferrari, M. Liscidini and F. G. Omenetto, *Adv. Mater.*, 2019, **31**, 1805312.
12 A. G. Dumanli and T. Savin, *Chem. Soc. Rev.*, 2016, **45**, 6698–6724.
13 A. I. Haines, C. E. Finlayson, D. R. E. Snoswell, P. Spahn, G. P. Hellmann and J. J. Baumberg, *Adv. Mater.*, 2012, **24**, 305–308.
14 J. Ge and Y. Yin, *Angew. Chem., Int. Ed.*, 2011, **50**, 1492–1522.
15 Y. Hu, Z. Tian, D. Ma, C. Qi, D. Yang and S. Huang, *Adv. Colloid Interface Sci.*, 2024, **324**, 103089.
16 Y. Qi and S. Zhang, *Smart Mol.*, 2023, **1**, e20230018.
17 T. Li, G. Liu, H. Kong, G. Yang, G. Wei and X. Zhou, *Coord. Chem. Rev.*, 2023, **475**, 214909.
18 K. Huang, Q. Li, Y. Xue, Q. Wang, Z. Chen and Z. Gu, *Adv. Drug Delivery Rev.*, 2023, **201**, 115075.
19 W. Wang, Y. Zhou, L. Yang, X. Yang, Y. Yao, Y. Meng and B. Tang, *Adv. Funct. Mater.*, 2022, **32**, 2204744.
20 C. Wang, C. Tang, Y. Wang, Y. Shen, W. Qi, T. Zhang, R. Su and Z. He, *Curr. Opin. Solid State Mater. Sci.*, 2022, **26**, 101017.
21 J. Wang, P. W. H. Pinkse, L. I. Segerink and J. C. T. Eijkel, *ACS Nano*, 2021, **15**, 9299–9327.
22 P. Wu, J. Wang and L. Jiang, *Mater. Horiz.*, 2020, **7**, 338–365.
23 Z.-J. Meng, J. Zhang, X. Deng, J. Liu, Z. Yu and C. Abell, *Mater. Horiz.*, 2019, **6**, 1938–1943.
24 W. Liu, H. Ma and A. Walsh, *Renewable Sustainable Energy Rev.*, 2019, **116**, 109436.
25 M. Li, X. Lai, C. Li and Y. Song, *Mater. Today Nano*, 2019, **6**, 100039.
26 M. Kuang, J. Wang and L. Jiang, *Chem. Soc. Rev.*, 2016, **45**, 6833–6854.
27 M. Kolle, P. M. Salgard-Cunha, M. R. Scherer, F. Huang, P. Vukusic, S. Mahajan, J. J. Baumberg and U. Steiner, *Nat. Nanotechnol.*, 2010, **5**, 511–515.
28 M. Li, Q. Lyu, B. Peng, X. Chen, L. Zhang and J. Zhu, *Adv. Mater.*, 2022, **34**, 2110488.
29 Z. Cai, Z. Li, S. Ravaine, M. He, Y. Song, Y. Yin, H. Zheng, J. Teng and A. Zhang, *Chem. Soc. Rev.*, 2021, **50**, 5898–5951.
30 S. Wu, H. Xia, J. Xu, X. Sun and X. Liu, *Adv. Mater.*, 2018, **30**, 1803362.
31 P. D. García, R. Sapienza, J. Bertolotti, M. D. Martín, Á. Blanco, A. Altube, L. Viña, D. S. Wiersma and C. López, *Phys. Rev. A:At., Mol., Opt. Phys.*, 2008, **78**, 023823.
32 D. S. Wiersma, *Nat. Photonics*, 2013, **7**, 188–196.
33 J. Lee, C. Y. Koh, J. P. Singer, S. Jeon, M. Maldovan, O. Stein and E. L. Thomas, *Adv. Mater.*, 2013, **26**, 532–569.
34 F. Meng, Z. Wang, S. Zhang, B. Ju and B. Tang, *Cell Rep. Phys. Sci.*, 2021, **2**, 100499.
35 L. Shi, Y. Zhang, B. Dong, T. Zhan, X. Liu and J. Zi, *Adv. Mater.*, 2013, **25**, 5314–5320.
36 G. Shang, M. Eich and A. Petrov, *APL Photonics*, 2020, **5**, 060901.
37 H. Noh, S. F. Liew, V. Saranathan, S. G. Mochrie, R. O. Prum, E. R. Dufresne and H. Cao, *Adv. Mater.*, 2010, **22**, 2871–2880.
38 G. Shang, L. Maiwald, H. Renner, D. Jalas, M. Dosta, S. Heinrich, A. Petrov and M. Eich, *Sci. Rep.*, 2018, **8**, 7804.
39 R. O. Prum, R. Torres, C. Kovach, S. Williamson and S. M. Goodman, *J. Exp. Biol.*, 1999, **202**, 3507–3522.
40 V. Hwang, A. B. Stephenson, S. Magkiriadou, J.-G. Park and V. N. Manoharan, *Phys. Rev. E*, 2020, **101**, 012614.
41 L. Schertel, L. Siedentop, J. M. Meijer, P. Keim, C. M. Aegerter, G. J. Aubry and G. Maret, *Adv. Opt. Mater.*, 2019, **7**, 1900442.
42 S. Magkiriadou, J.-G. Park, Y.-S. Kim and V. N. Manoharan, *Phys. Rev. E:Stat., Nonlinear, Soft Matter Phys.*, 2014, **90**, 062302.
43 E. R. Dufresne, H. Noh, V. Saranathan, S. G. J. Mochrie, H. Cao and R. O. Prum, *Soft Matter*, 2009, **5**, 1792–1795.
44 L. Maiwald, S. Lang, D. Jalas, H. Renner, A. Y. Petrov and M. Eich, *Opt. Express*, 2018, **26**, 11352.
45 N. Vogel, S. Utech, G. T. England, T. Shirman, K. R. Phillips, N. Koay, I. B. Burgess, M. Kolle, D. A. Weitz and J. Aizenberg, *Proc. Natl. Acad. Sci. U. S. A.*, 2015, **112**, 10845–10850.
46 Y. Takeoka, S. Yoshioka, A. Takano, S. Arai, K. Nueangnoraj, H. Nishihara, M. Teshima, Y. Ohtsuka and T. Seki, *Angew. Chem., Int. Ed.*, 2013, **52**, 7261–7265.
47 L. Song, X. Chen, Y. Xie, L. Zhong, X. Zhang and Z. Cheng, *Dyes Pigm.*, 2019, **164**, 222–226.
48 P. Colson, R. Cloots and C. Henrist, *Langmuir*, 2011, **27**, 12800–12806.
49 J. D. Förster, H. Noh, S. F. Liew, V. Saranathan, C. F. Schreck, L. Yang, J. G. Park, R. O. Prum, S. G. Mochrie, C. S. O'Hern, H. Cao and E. R. Dufresne, *Adv. Mater.*, 2010, **22**, 2939–2944.
50 Y. Zhang, B. Dong, A. Chen, X. Liu, L. Shi and J. Zi, *Adv. Mater.*, 2015, **27**, 4719–4724.
51 L. Bai, Y. Lim, J. Zhou, L. Liang and H. Duan, *Langmuir*, 2019, **35**, 9878–9884.
52 B. Yi and H. Shen, *J. Mater. Chem. C*, 2017, **5**, 8194–8200.
53 L. Bai, V. C. Mai, Y. Lim, S. Hou, H. Mohwald and H. Duan, *Adv. Mater.*, 2018, **30**, 1705667.
54 V. T. Tran, J. Kim, S. Oh, K. J. Jeong and J. Lee, *Small*, 2022, **18**, 2200317.
55 J. Zhang, J. Zhang, Y. Ou, Y. Qin, H. Wen, W. Dong, R. Wang, S. Chen and Z. Yu, *Small*, 2021, **17**, 2007426.
56 H. Tan, Q. Lyu, Z. Xie, M. Li, K. Wang, K. Wang, B. Xiong, L. Zhang and J. Zhu, *Adv. Mater.*, 2019, **31**, 1805496.
57 J. Zhou, P. Han, M. Liu, H. Zhou, Y. Zhang, J. Jiang, P. Liu, Y. Wei, Y. Song and X. Yao, *Angew. Chem., Int. Ed.*, 2017, **56**, 10462–10466.
58 M. Li, H. Tan, L. Jia, R. Zhong, B. Peng, J. Zhou, J. Xu, B. Xiong, L. Zhang and J. Zhu, *Adv. Funct. Mater.*, 2020, **30**, 2000008.
59 Y. Zhang, P. Han, H. Zhou, N. Wu, Y. Wei, X. Yao, J. Zhou and Y. Song, *Adv. Funct. Mater.*, 2018, **28**, 1802585.
60 Y. Liu, C. Shao, Y. Wang, L. Sun and Y. Zhao, *Matter*, 2019, **1**, 1581–1591.
61 F. Meng, M. M. Umair, K. Iqbal, X. Jin, S. Zhang and B. Tang, *ACS Appl. Mater. Interfaces*, 2019, **11**, 13022–13028.

62 L. Zhou, J. Fei, W. Fang, L. Shao, Q. Liu, H. He, M. Ma, Y. Shi, S. Chen and X. Wang, *Nanoscale Horiz.*, 2022, **7**, 890–898.
63 Z. Hu, N. P. Bradshaw, B. Vanthournout, C. Forman, K. Gnanasekaran, M. P. Thompson, P. Smeets, A. Dhinojwala, M. D. Shawkey, M. C. Hersam and N. C. Gianneschi, *Chem. Mater.*, 2021, **33**, 6433–6442.
64 S.-H. Kim, J.-M. Lim, W. C. Jeong, D.-G. Choi and S.-M. Yang, *Adv. Mater.*, 2008, **20**, 3211–3217.
65 R. Shanker, S. Sardar, S. Chen, S. Gamage, S. Rossi and M. P. Jonsson, *Nano Lett.*, 2020, **20**, 7243–7250.
66 L. Siegwardt and M. Gallei, *Adv. Funct. Mater.*, 2023, **33**, 2213099.
67 Q. Guo, X. Wang, J. Guo and C. Wang, *Nanoscale*, 2023, **15**, 18825–18831.
68 J. M. Clough, E. Guimard, C. Rivet, J. Sprakel and T. E. Kodger, *Adv. Opt. Mater.*, 2019, **7**, 1900218.
69 M. Xiao, Z. Y. Hu, Z. Wang, Y. W. Li, A. D. Tormo, N. L. Thomas, B. X. Wang, N. C. Gianneschi, M. D. Shawkey and A. Dhinojwala, *Sci. Adv.*, 2017, **3**, e1701151.
70 Y. Zhao, L. Shang, Y. Cheng and Z. Gu, *Acc. Chem. Res.*, 2014, **47**, 3632–3642.
71 Z. Yu, C. F. Wang, L. Ling, L. Chen and S. Chen, *Angew. Chem., Int. Ed.*, 2012, **51**, 2375–2378.
72 J. G. Park, S. H. Kim, S. Magkiriadou, T. M. Choi, Y. S. Kim and V. N. Manoharan, *Angew. Chem., Int. Ed.*, 2014, **53**, 2899–2903.
73 L. Torres, A. Margaronis, B. M. Bellato Meinhardt, L. Granzow, O. B. Ayyub and P. Kofinas, *Langmuir*, 2020, **36**, 1252–1257.
74 Z. Lin, Z. Gong, D. Q. Bower, D. Lee and L. F. Deravi, *Adv. Opt. Mater.*, 2021, **9**, 2100416.
75 W. Yu, Y. Zhao, W. Sheng and J. Ge, *Adv. Funct. Mater.*, 2023, **33**, 2304474.
76 I. Lee, D. Kim, J. Kal, H. Baek, D. Kwak, D. Go, E. Kim, C. Kang, J. Chung, Y. Jang, S. Ji, J. Joo and Y. Kang, *Adv. Mater.*, 2010, **22**, 4973–4977.
77 J. Han, E. Lee, J. K. Dudoff, M. Bagge-Hansen, J. R. I. Lee, A. J. Pascall, J. D. Kuntz, T. M. Willey, M. A. Worsley and T. Y. J. Han, *Adv. Opt. Mater.*, 2017, **5**, 1600838.
78 K. Katagiri, Y. Tanaka, K. Uemura, K. Inumaru, T. Seki and Y. Takeoka, *NPG Asia Mater.*, 2017, **9**, e355–e355.
79 Q. Zhao, C. E. Finlayson, D. R. Snoswell, A. Haines, C. Schafer, P. Spahn, G. P. Hellmann, A. V. Petukhov, L. Herrmann, P. Burdet, P. A. Midgley, S. Butler, M. Mackley, Q. Guo and J. J. Baumberg, *Nat. Commun.*, 2016, **7**, 11661.
80 M. Sakai, H. Kim, Y. Arai, T. Teratani, Y. Kawai, Y. Kuwahara, K. Abe, Y. Kuwana, K. Ikeda, K. Yamada and Y. Takeoka, *ACS Appl. Nano Mater.*, 2020, **3**, 7047–7056.
81 M. Xiao, Y. Li, M. C. Allen, D. D. Deheyn, X. Yue, J. Zhao, N. C. Gianneschi, M. D. Shawkey and A. Dhinojwala, *ACS Nano*, 2015, **9**, 5454.
82 X. Yang, D. Ge, G. Wu, Z. Liao and S. Yang, *ACS Appl. Mater. Interfaces*, 2016, **8**, 16289–16295.
83 M. Shaban, A. M. Ahmed, E. Abdel-Rahman and H. Hamdy, *Sci. Rep.*, 2017, **7**, 41983.
84 Y. Takeoka, S. Yoshioka, A. Takano, S. Arai, K. Nueangnoraj, H. Nishihara, M. Teshima, Y. Ohtsuka and T. Seki, *Angew. Chem., Int. Ed.*, 2013, **52**, 7261–7265.
85 Y. Han, Z. Meng, Y. Wu, S. Zhang and S. Wu, *ACS Appl. Mater. Interfaces*, 2021, **13**, 57796–57802.
86 B. Q. Dong, X. H. Liu, T. R. Zhan, L. P. Jiang, H. W. Yin, F. Liu and J. Zi, *Opt. Express*, 2010, **18**, 14430.
87 J. A. H. P. Sol, H. Sentjens, L. Yang, N. Grossiord, A. P. H. J. Schenning and M. G. Debije, *Adv. Mater.*, 2021, **33**, 2103309.
88 A. T. L. Tan, S. Nagelberg, E. Chang-Davidson, J. Tan, J. K. W. Yang, M. Kolle and A. J. Hart, *Small*, 2020, **16**, 1905519.
89 A. T. L. Tan, J. Beroz, M. Kolle and A. J. Hart, *Adv. Mater.*, 2018, **30**, 1803620.
90 J. B. Kim, C. J. Chae, S. H. Han, S. Y. Lee and S. H. Kim, *Sci. Adv.*, 2021, **7**, eabj8780.
91 M. Kuang, J. Wang, B. Bao, F. Li, L. Wang, L. Jiang and Y. Song, *Adv. Opt. Mater.*, 2013, **2**, 34–38.
92 K. Li, T. Li, T. Zhang, H. Li, A. Li, Z. Li, X. Lai, X. Hou, Y. Wang, L. Shi, M. Li and Y. Song, *Sci. Adv.*, 2021, **7**, eabh1992.
93 Y. Zhang, L. Zhang, C. Zhang, J. Wang, J. Liu, C. Ye, Z. Dong, L. Wu and Y. Song, *Nat. Commun.*, 2022, **13**, 7095.
94 J. Liao, C. Ye, J. Guo, C. E. Garciamendez-Mijares, P. Agrawal, X. Kuang, J. O. Japo, Z. Wang, X. Mu, W. Li, T. Ching, L. S. Mille, C. Zhu, X. Zhang, Z. Gu and Y. S. Zhang, *Mater. Today*, 2022, **56**, 29–41.
95 Y. Liu, H. Wang, J. Ho, R. C. Ng, R. J. H. Ng, V. H. Hall-Chen, E. H. H. Koay, Z. Dong, H. Liu, C.-W. Qiu, J. R. Greer and J. K. W. Yang, *Nat. Commun.*, 2019, **10**, 4340.
96 S. H. Han, Y. H. Choi and S. H. Kim, *Small*, 2021, **18**, 2106048.
97 S. Park, H. Hwang, M. Kim, J. H. Moon and S.-H. Kim, *Nanoscale*, 2020, **12**, 18576–18594.
98 D. Liu, F. Zhou, C. Li, T. Zhang, H. Zhang, W. Cai and Y. Li, *Angew. Chem., Int. Ed.*, 2015, **54**, 9596–9600.
99 S. K. Nam, J. B. Kim, S. H. Han and S. H. Kim, *ACS Nano*, 2020, **14**, 15714–15722.
100 G. H. Lee, S. H. Han, J. B. Kim, D. J. Kim, S. Lee, W. M. Hamonangan, J. M. Lee and S.-H. Kim, *ACS Appl. Polym. Mater.*, 2019, **2**, 706–714.
101 T. M. Choi, G. H. Lee, Y. S. Kim, J. G. Park, H. Hwang and S. H. Kim, *Adv. Mater.*, 2019, **31**, e1900693.
102 S. S. Lee, S. K. Kim, J. C. Won, Y. H. Kim and S. H. Kim, *Angew. Chem., Int. Ed.*, 2015, **54**, 15266–15270.
103 J. Wang and J. Zhu, *Eur. Polym. J.*, 2013, **49**, 3420–3433.
104 M. Zhu, H. Li, Q. Guo, J. Guo and C. Wang, *ACS Appl. Mater. Interfaces*, 2024, **16**, 32543–32553.
105 Q. Fu, W. Yu, G. Bao and J. Ge, *Nat. Commun.*, 2022, **13**, 7007.
106 K. Katagiri, K. Uemura, R. Uesugi, N. Tarutani, K. Inumaru, T. Uchikoshi, T. Seki and Y. Takeoka, *ACS Appl. Mater. Interfaces*, 2020, **12**, 40768–40777.
107 X. Xu, Z. Liu, Y. Liu, X. Zhang, Z. Zheng, D. Luo and X. Sun, *Adv. Opt. Mater.*, 2017, **6**, 1700891.

108 X. Wang, X. Liang, Y. Li, X. Li, G. Liu, M. Hu, Y. Liu, Y. Huang, L. Zhou, W. Zhou and J. Shao, *Chem. Eng. J.*, 2024, **483**, 149053.
109 M. Li, B. Peng, Q. Lyu, X. Chen, Z. Hu, X. Zhang, B. Xiong, L. Zhang and J. Zhu, *Nat. Commun.*, 2024, **15**, 1874.
110 Y. Li, Q. Fan, X. Wang, G. Liu, L. Chai, L. Zhou, J. Shao and Y. Yin, *Adv. Funct. Mater.*, 2021, **31**, 2010746.
111 Y. Wang, P. Kanjanaboos, S. P. McBride, E. Barry, X. M. Lin and H. M. Jaeger, *Faraday Discuss.*, 2015, **181**, 325–338.
112 T. H. Besseling, M. Hermes, A. Fortini, M. Dijkstra, A. Imhof and A. van Blaaderen, *Soft Matter*, 2012, **8**, 6931.
113 Q. Guo, S. Chen, H. Li, X. Wang, J. He, J. Chu, J. Guo and C. Wang, *Chem. Eng. J.*, 2024, **488**, 150969.
114 G. Jacucci, S. Vignolini and L. Schertel, *Proc. Natl. Acad. Sci. U. S. A.*, 2020, **117**, 23345–23349.
115 M. Iwata, M. Teshima, T. Seki, S. Yoshioka and Y. Takeoka, *Adv. Mater.*, 2017, **29**, 1605050.
116 B. Yi and H. Shen, *Chem. Commun.*, 2017, **53**, 9234–9237.
117 S. Zhang, J. Liu, X. Wang, D. Liu, Q. Tian, H. Shen, J. Zhang, D. Song, W. Dong and Z. Yu, *Chem. Eng. Sci.*, 2024, **298**, 120398.
118 X. Chen, D.-P. Song and Y. Li, *Macromolecules*, 2022, **55**, 7438–7445.
119 Y. Ohtsuka, T. Seki and Y. Takeoka, *Angew. Chem., Int. Ed.*, 2015, **54**, 15368–15373.
120 G. H. Lee, J. Y. Sim and S.-H. Kim, *ACS Appl. Mater. Interfaces*, 2016, **8**, 12473–12480.
121 S.-H. Kim, S. Magkiriadou, D. K. Rhee, D. S. Lee, P. J. Yoo, V. N. Manoharan and G.-R. Yi, *ACS Appl. Mater. Interfaces*, 2017, **9**, 24155–24160.
122 Q. He, H. Vijayamohanan, J. Li and T. M. Swager, *J. Am. Chem. Soc.*, 2022, **144**, 5661–5667.
123 J. Kim, H. Yun, Y. J. Lee, J. Lee, S. H. Kim, K. H. Ku and B. J. Kim, *J. Am. Chem. Soc.*, 2021, **143**, 13333–13341.
124 E. J. Kim, J. J. Shin, T. Do, G. S. Lee, J. Park, V. Thapar, J. Choi, J. Bang, G. R. Yi, S. M. Hur, J. G. Kim and B. J. Kim, *ACS Nano*, 2021, **15**, 5513–5522.
125 Q. Guo, Y. Li, Q. Liu, Y. Li and D. P. Song, *Angew. Chem., Int. Ed.*, 2022, **61**, e202113759.
126 Y. Dong, Z. Ma, D.-P. Song, G. Ma and Y. Li, *ACS Nano*, 2021, **15**, 8770–8779.
127 J. J. Shin, E. J. Kim, K. H. Ku, Y. J. Lee, C. J. Hawker and B. J. Kim, *ACS Macro Lett.*, 2020, **9**, 306–317.
128 Q. He, K. H. Ku, H. Vijayamohanan, B. J. Kim and T. M. Swager, *J. Am. Chem. Soc.*, 2020, **142**, 10424–10430.
129 D. P. Song, T. H. Zhao, G. Guidetti, S. Vignolini and R. M. Parker, *ACS Nano*, 2019, **13**, 1764–1771.
130 J. Lee, K. H. Ku, J. Kim, Y. J. Lee, S. G. Jang and B. J. Kim, *J. Am. Chem. Soc.*, 2019, **141**, 15348–15355.
131 Y. Yang, H. Kim, J. Xu, M. S. Hwang, D. Tian, K. Wang, L. Zhang, Y. Liao, H. G. Park, G. R. Yi, X. Xie and J. Zhu, *Adv. Mater.*, 2018, **30**, 1707344.
132 K. H. Ku, J. M. Shin, D. Klinger, S. G. Jang, R. C. Hayward, C. J. Hawker and B. J. Kim, *ACS Nano*, 2016, **10**, 5243–5251.
133 Q.-J. Liu, Y. Li, J.-C. Xu, H.-F. Lu, Y. Li and D.-P. Song, *ACS Nano*, 2021, **15**, 5534–5544.
134 X. Chen, X. Yang, D.-P. Song, Y.-F. Men and Y. Li, *Macromolecules*, 2021, **54**, 3668–3677.
135 Y. L. Li, X. Chen, H. K. Geng, Y. Dong, B. Wang, Z. Ma, L. Pan, G. Q. Ma, D. P. Song and Y. S. Li, *Angew. Chem., Int. Ed.*, 2020, **60**, 3647–3653.
136 X. Li, B. Xia, Y. Song, M. Zheng, C. Huang, Y. Li and D. Song, *Macromolecules*, 2024, **57**, 7915–7925.
137 D. Liu, Z. Zhang, K. Zhang, Y. Li and D. Song, *Small*, 2024, **20**, 2312099.
138 T. H. Zhao, G. Jacucci, X. Chen, D. P. Song, S. Vignolini and R. M. Parker, *Adv. Mater.*, 2020, **32**, 2002681.
139 Z. Wang, R. Li, Y. Zhang, C. L. C. Chan, J. S. Haataja, K. Yu, R. M. Parker and S. Vignolini, *Adv. Mater.*, 2023, **35**, 2207923.
140 G. Shang, L. Maiwald, H. Renner, D. Jalas, M. Dosta, S. Heinrich, A. Petrov and M. Eich, *Sci. Rep.*, 2018, **8**, 7804.
141 L. Maiwald, S. Lang, D. Jalas, H. Renner, A. Y. Petrov and M. Eich, *Opt. Express*, 2018, **26**, 11352.
142 Q. Zhong, Z. Xie, H. Ding, C. Zhu, Z. Yang and Z. Gu, *Small*, 2015, **11**, 5766–5770.
143 X. Zhao, Y. Cao, F. Ito, H. H. Chen, K. Nagai, Y. H. Zhao and Z. Z. Gu, *Angew. Chem., Int. Ed.*, 2006, **45**, 6835–6838.
144 J. H. Moon, G. R. Yi, S. M. Yang, D. J. Pine and S. B. Park, *Adv. Mater.*, 2004, **16**, 605–609.
145 J. S. Foresi, P. R. Villeneuve, J. Ferrera, E. R. Thoen, G. Steinmeyer, S. Fan, J. D. Joannopoulos, L. C. Kimerling, H. I. Smith and E. P. Ippen, *Nature*, 1997, **390**, 143–145.
146 X. Su, H. Xia, S. Zhang, B. Tang and S. Wu, *Nanoscale*, 2017, **9**, 3002–3009.
147 J. Bi, S. Wu, H. Xia, L. Li and S. Zhang, *J. Mater. Chem. C*, 2019, **7**, 4551–4558.
148 J. Tan, J. Sun, T. Ye, H. Liu, J. Liu and C. Wang, *ACS Appl. Mater. Interfaces*, 2024, **16**, 41300–41309.
149 S. Wu, J. Nan, Y. Wu, Z. Meng and S. Zhang, *ACS Appl. Mater. Interfaces*, 2022, **14**, 27048–27055.
150 F. Wang, Y. Xue, B. Lu, H. Luo and J. Zhu, *Langmuir*, 2019, **35**, 4918–4926.
151 F. Wang, X. Zhang, Y. Lin, L. Wang and J. Zhu, *ACS Appl. Mater. Interfaces*, 2016, **8**, 5009–5016.
152 L. Schertel, I. Wimmer, P. Besirske, C. M. Aegerter, G. Maret, S. Polarz and G. J. Aubry, *Phys. Rev. Mater.*, 2019, **3**, 015203.
153 G. J. Aubry, L. Schertel, M. Chen, H. Weyer, C. M. Aegerter, S. Polarz, H. Cölfen and G. Maret, *Phys. Rev. A*, 2017, **96**, 043871.
154 H. Noh, S. F. Liew, V. Saranathan, R. O. Prum, S. G. J. Mochrie, E. R. Dufresne and H. Cao, *Phys. Rev. E:Stat., Nonlinear, Soft Matter Phys.*, 2010, **81**, 051923.
155 C. M. Heil, A. Patil, B. Vanthournout, S. Singla, M. Bleuel, J. Song, Z. Hu, N. C. Gianneschi, M. D. Shawkey, S. K. Sinha, A. Jayaraman and A. Dhinojwala, *Sci. Adv.*, 2023, **9**, eadf2859.
156 G. Shang, L. Maiwald, H. Renner, D. Jalas, M. Dosta, S. Heinrich, A. Petrov and M. Eich, *Sci. Rep.*, 2018, **8**, 7804.
157 S. Zhao, H. Zhu, J. Lu, M. Li, L. Zhao, L. Zhou and L. Gao, *Adv. Funct. Mater.*, 2022, **32**, 2201927.
158 B. E. Droguet, H.-L. Liang, B. Frka-Petesic, R. M. Parker, M. F. L. De Volder, J. J. Baumberg and S. Vignolini, *Nat. Mater.*, 2021, **21**, 352–358.

159 M. Xu, X. Wu, Y. Yang, C. Ma, W. Li, H. Yu, Z. Chen, J. Li, K. Zhang and S. Liu, *ACS Nano*, 2020, **14**, 11130–11139.
160 Q. Guo, R. Xue, J. Zhao, Y. Zhang, G. T. van de Kerkhof, K. Zhang, Y. Li, S. Vignolini and D. P. Song, *Angew. Chem., Int. Ed.*, 2022, **61**, e202206723.
161 J. Chu, Y. Chen, S. Y. Tan, Y. Y. Liu, W. Liu, X. Liu, L. Shi, H. Wang, W. Li and J. Zi, *Adv. Opt. Mater.*, 2021, **10**, 2102125.
162 S. Ming, X. Zhang, C. L. C. Chan, Z. Wang, M. M. Bay, R. M. Parker and S. Vignolini, *Adv. Sustainable Syst.*, 2023, **7**, 2200469.